Editors' Suggestion

# Frustrated Kondo impurity triangle: A simple model of deconfinement

Elio J. König,[1,2,*] Piers Coleman,[1,3] and Yashar Komijani[1,4]

[1]*Department of Physics and Astronomy, Center for Materials Theory, Rutgers University, Piscataway, New Jersey 08854, USA*
[2]*Max Planck Institute for Solid State Research, Heisenbergstraße 1, 70569 Stuttgart, Germany*
[3]*Department of Physics, Royal Holloway, University of London, Egham, Surrey TW20 0EX, United Kingdom*
[4]*Department of Physics, University of Cincinnati, Cincinnati, Ohio 45221-0011, USA*

(Received 4 December 2020; revised 25 June 2021; accepted 16 July 2021; published 3 September 2021)

The concepts of deconfinement and topological order are of great current interest for quantum information science and for our understanding of quantum materials. Here, we introduce a simple model of three antiferromagnetically coupled Kondo impurities, a *Kondo triangle*, which can be used to further extend the application of these concepts to electronic systems. We show that, by tuning the magnetic frustration, the Kondo triangle undergoes a quantum phase transition between two phases of unbroken symmetry, signaling a phase transition beyond the Landau paradigm. We demonstrate that the frustrated spin liquid phase is described by a three-channel Kondo (3CK) fixed point and thus displays an irrational ground state degeneracy. Using an Abrikosov pseudofermion representation, this quantum state is categorized by an emergent $U(1)$ gauge field and its projective symmetry group. The gauge theory is deconfining in the sense that a miniature Wilson loop orders and topological defects (instantons in the gauge field) are expelled. This phase persists in the presence of moderate Kondo screening until proliferation of topological defects leads to a quantum phase transition to an unfrustrated Fermi liquid phase. Based on this evidence, we propose that the 3CK phase displays topological order in a similar sense as gapless spin liquids.

DOI: 10.1103/PhysRevB.104.115103

## I. INTRODUCTION

Recent discoveries in quantum materials have urged us to generalize Landau's notion of broken symmetry by introducing classes of quantum order without symmetry breaking. The prime example is quantum magnetism in which strong frustration can give rise to quantum spin liquids (QSLs) [1,2] with fractionalized quasiparticles, patterns of long-range entanglement, and topological order [3]. Similar physics occurs at continuous phase transitions between ordered phases with different symmetries which require a fractionalized description (*deconfined criticality*) [4].

These ideas are of particular relevance to doped QSLs in the vicinity of Mott delocalization, a topic of potential importance for cuprate [5], organic salts [6,7], and iron-based [8] high-$T_c$ superconductors. A closely related topic is the interaction of electrons and spin liquids via a Kondo interaction, as in geometrically frustrated heavy fermion compounds (e.g., CePdAl [9,10]), transition metal dichalcogenides (e.g., 4Hb-$TaS_2$ [11]), and in engineered van der Waals heterostructures of graphene and $RuCl_3$ [12].

A significant component of this intriguing physics is thought to involve the fractionalization of spins [13,14] into *spinons*, fractionalized particles interacting with an emergent gauge field. Fractionalization is a useful concept if the emergent gauge theory is in the deconfining phase. In two- (2D) plus one-dimensional (1D) compact quantum electrodynamics ($QED_3$), deconfinement is lost via a proliferation of instantons in the gauge field [15], but the presence of fermions [16–20] counteracts this mechanism allowing for a confinement-deconfinement quantum phase transition. It has been argued that transitions out of spin-liquid phases via partial Mott delocalization, e.g., in heavy-fermion materials, lead to a Fermi surface reconstruction that may be understood in these terms [21–23].

In addition to its importance for quantum materials, deconfinement of anyonic quasiparticles is of prime importance

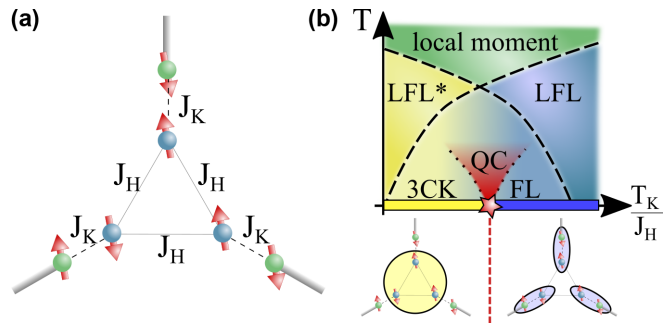


FIG. 1. (a) An antiferromagnetic triangle, where each spin is coupled to its own conduction bath, caricatures a spin-liquid competing with a Fermi liquid (FL). (b) When $T_K/J_H$ is large, each spin is individually Kondo screened [local FL (LFL), right inset]. In contrast, at the smallest $T_K/J_H$, the ground state manifold of the impurity forms an effective spin (left inset), and the system develops a three-channel Kondo (3CK) phase, in which instantons of the emergent gauge theory are irrelevant. Analogously to confinement in two- plus one-dimensional quantum electrodynamics ($QED_3$), instantons proliferate beyond a critical $T_K/J_H$ (red star) and restore an ordinary (L)FL.

*elio.j.koenig@gmail.com

 

for topological quantum computation [24], which may be realized in materials (as discussed above) or by artificially interweaving nontopological qubits into robust, macroscopic logical qubits, e.g., within the surface code. As it appears particularly desirable to *electronically* manipulate and braid the emergent excitations, a natural important question regards when and how topological order is destroyed by the coupling to electronic leads.

Related phenomena appear in the context of magnetic impurities, as in the overscreened Kondo effect [25–29], and in magnetically frustrated Kondo screened impurities [30–34]. The frustration leads to the fractionalization of the spin and an irrational residual entropy suggestive of non-Abelian anyons [35] which is potentially useful as a platform for topological quantum computation [36,37]. The common theme of these systems is an abundance of competing patterns of spin entanglement and their rearrangement at a quantum critical point (QCP).

Here, we investigate a *Kondo triangle model* involving three antiferromagnetically coupled spins at the vertices of a triangle, each independently coupled to its own conduction sea [Fig. 1(a)] [38,39]. The solvable limits of this model enable us to demonstrate a transition between two distinct ground states (phases) without any symmetry breaking. In one of these two phases, each spin is Kondo screened separately, and the spins are not mutually entangled. In the other phase, the spins are strongly entangled and the coupling to the leads results in an irrational impurity entropy. To gain a better insight, we have explored the physics of a Kondo triangle near the large $N$ limit of spins with an $SU(N)$ symmetry. Our procedure contains three steps:

(i) We prefractionalize spins in terms of Abrikosov fermion "spinons" [40]. (ii) Decoupling of interactions leads to a quadratic Hamiltonian [41] with a $U(1)$ flux $\Phi$ through the triangle. (iii) We go beyond mean-field theory by studying $1/N$ corrections and the nonperturbative effects of instantons (i.e., phase slips $\Phi \to \Phi \pm 2\pi$).

The presence of these phase slips makes the problem distinct from the two-impurity Kondo problem discussed extensively in the past [28,42–44] and allows us to draw analogies to the confinement mechanism in $QED_3$ and to fractionalization in $2+1$D quantum materials in general.

We conclude this introduction with an overview of previous works on confinement-deconfinement quantum phase transitions in Kondo lattice systems. Senthil *et al.* [21,45] introduced the concept of fractionalized Fermi liquid (FL$^*$) phases, in which the Kondo screening of lattice spins breaks down at the expense of establishing a QSL in the spin system. When the latter is a $\mathbb{Z}_2$ QSL, the FL$^*$ is particularly robust, but FL$^*$ and ordinary Fermi liquid (FL) are separated by a superconducting phase which breaks particle number conservation. In contrast, the transition from an FL$^*$ with $U(1)$ QSL to the Kondo screened FL may be direct, does not involve the breaking of any microscopic symmetries, and is governed by a QCP [45–47]. To study this phase transition in low-dimensional Kondo problems, a study of fermionic degrees of freedom coupled to compact gauge fields seems essential to stabilize deconfinement.

The remainder of this paper is structured as follows: In Sec. II, we define the model under consideration and summarize the main results. Section III contains a mapping of the triangle model to a three-channel Kondo (3CK) model which is independent of the approximate large-$N$ treatment introduced in Sec. IV. Fluctuation corrections beyond the $N \to \infty$ limit are discussed in Sec. V, while the conclusions, Sec. VI, contain a discussion of the relationship to topological order and of the experimental implications of this paper.

## II. MODEL AND SUMMARY OF RESULTS

### A. Model Hamiltonian

The Kondo triangle Hamiltonian [Fig. 1(a)] $H = H_c + H_{\rm H} + H_{\rm K}$ consists of three terms:

$$H_c = \sum_{m=1}^{3} \sum_{\mathbf{p}} \tilde{c}^\dagger_{\alpha,m}(\mathbf{p}) \epsilon(\mathbf{p}) \tilde{c}_{\alpha,m}(\mathbf{p}), \tag{1a}$$

$$H_{\rm H} = \frac{J_{\rm H}}{N} \sum_{m=1}^{3} \hat{S}^a_m \hat{S}^a_{m+1}, \tag{1b}$$

$$H_{\rm K} = \frac{J_{\rm K}}{N} \sum_{m=1}^{3} \hat{S}^a_m c^\dagger_{\alpha,m}(0) \sigma^a_{\alpha\beta} c_{\beta,m}(0). \tag{1c}$$

The operators $c^\dagger_m(\mathbf{x})$ [$\tilde{c}^\dagger_m(\mathbf{p}) = \sum_x e^{-i\mathbf{p}\cdot\mathbf{x}} c^\dagger_m(\mathbf{x})$] create electrons on lead $m$, with a dispersion $\epsilon(\mathbf{p})$. The $\sigma^a$ ($a = 1 \ldots N^2 - 1$) are generators of the fundamental representation of $SU(N)$, and $\hat{S}^a_m$ are the corresponding spin operators. Summation convention over repeated spin indices $\alpha, \beta = 1, \ldots, N$ is implied, but summations over the lead index $m$ are written explicitly. In this paper, we will mainly use the Abrikosov fermion representation of spins $\hat{S}^a_m = f^\dagger_{\alpha,m}(\sigma^a)_{\alpha\beta} f_{m,\beta}$, with the constraint $f^\dagger_{\alpha,m} f_{\alpha,m} = Q$, where $Q = Nq$.

### B. Comparison to previous works

For a large Kondo temperature $T_{\rm K} = De^{-1/J_{\rm K}\rho} \gg J_{\rm H}$, the model yields a local FL (LFL), see Fig. 1(b), in which each spin is magnetically screened by its own conduction band. The situation is more intricate for small $T_{\rm K} \ll J_{\rm H}$. For $SU(2)$ spins, Ferrero *et al.* [38] employed a combination of conformal field theory and numerical renormalization group to demonstrate that the LFL phase is stable at all values of the ratio $T_{\rm K}/J_{\rm H}$. Recently, we investigated the ferromagnetic version [48] of Eq. (1) which has a FL ground state for all parameters.

However, $C_3$ symmetric models of spin-$\frac{1}{2}$ triangles, which are Kondo coupled [49] to a single 2D or 3D electronic bath, were considered by Lazarovits *et al.* [32] using a renormalization group approach. Contrary to Eq. (1), this setup features substantial intersite correlations $\langle c^\dagger_{\alpha,m}(\tau) c_{\alpha,m+1}(0)\rangle$ which can lead to an exotic non-FL fixed point. The model was studied numerically by Paul and Ingersent [50] and analytically by Ingersent *et al.* [30]. Very recently, Eickhoff and Anders [51] have revisited the model with the goal of developing a cluster dynamical mean-field theory.

Finally, a vast amount of literature is devoted to asymmetric triangles in which Kondo coupling to the leads is site selective and/or the Heisenberg interaction is not homogeneous, see, e.g., Refs. [33,52,53].

### C. Summary of results

In this paper, we generalize this model beyond $SU(2)$ to the case of spins forming an antisymmetric representation of $SU(N)$, described by vertical Young tableaux with $Q$ boxes. In Sec. III, we show that, for a sequence of $(N, Q)$, our model at smallest $T_K/J_H$ maps onto a single composite spin, overscreened by three conduction channels, denoted here as 3CK. This solvable limit corresponds to a phase with a nontrivial ground state degeneracy, differing from the LFL at large $T_K/J_H$. However, neither phase breaks any symmetries of the model.

Within the large-$N$ approach, the appearance of spinons is accompanied by an emergent $U(1)$ gauge field on the links of the triangle, with a gauge invariant flux $\oint \vec{A} \cdot d\vec{x} = \Phi$ that threads the triangle. The 3CK phase [Fig. 1(b)], is characterized by the ordering of the symmetric ring exchange operator

$$\mathcal{O}_s \equiv d_{abc} \hat{S}_1^a \hat{S}_2^b \hat{S}_3^c \propto \cos(\Phi), \quad d_{abc} \equiv \mathrm{tr}[\sigma^a \{\sigma^b, \sigma^c\}], \quad (2)$$

which preserves time reversal, spin $SU(N)$, and crystalline $C_{3v}$ symmetries.

By contrast, in the FL, phase slips proliferate, confining the spinons to each lead, and in this sense, the two phases are separated by a confinement-deconfinement transition. Both (FL and 3CK) phases are robust against deformations of the triangle (i.e., unequal $J_H$), which make them suitable for future experimental realizations.

Finally, we comment on special values of $Q$ and $N$. First, the particle-hole symmetric representation $Q/N = \frac{1}{2}$, which is related to $SU(2)$ spins, has mean-field solutions for which some of the links are missing and the flux is ill defined [see Fig. 3(a), below]. Moreover, the order parameter $\mathcal{O}_s$ of the 3CK phase vanishes for $N = 2$ since $d_{abc} = 0$ for $SU(2)$ spins. These arguments explain the persistence of the FL phase down to $T_K/J_H \to 0$ for the $SU(2)$ triangle [38].

Second, at commensurate representations $Q = N/3$, or $Q = 2N/3$, the spins form a singlet at small $T_K/J_H$, and the competition between Heisenberg and Kondo interactions is analogous to the $SU(2)$ two-impurity two-channel Kondo problem, i.e., the two limiting phases are FLs with conduction electron phase shift of $\delta_c = 0, \pi$. For these commensurate representations, instead of the 3CK phase, we have a FL$^*$, i.e., a gapped spin-liquid which is robust to the Kondo interaction up to a threshold coupling, and a FL$^*$-to-FL transition.

## III. MAPPING TO 3CK MODELS

We first highlight a subset of models, with $N = 3Q + 1$, of which the simplest is the fundamental representation of $SU(4)$. In these special cases, we can show that 3CK behavior develops at large $J_H$. To see this, we first solve $H_H$ at $J_K = 0$. It is convenient to employ the previously introduced Abrikosov fermion representation of the spin, and we emphasize that, here, no approximations are made (for details, see Appendix A). The antiferromagnetic coupling $J_H$ favors the formation of a maximally antisymmetrized combination of $3Q$ spinons. Since $3Q = N - 1$, this system is one spinon short of an overall $SU(N)$ singlet. Indeed, if one of the spins, say $m$, had a larger representation, i.e., $Q + 1$ (rather than $Q$) vertical boxes, the three spins could form a singlet, denoted by $|\text{singlet}, m\rangle$. When all spins have representation $Q$, the ground state of the Heisenberg Hamiltonian $H_H$ can be shown (Appendix A 2) to be

$$|\alpha\rangle = \frac{1}{\sqrt{3}} \sum_m f_{m,\alpha} |\text{singlet}, m\rangle, \quad (3)$$

where $\alpha = 1 \ldots N$ and states $\{|\alpha\rangle\}$ form a basis for the conjugate representation of $SU(N)$. The corresponding matrix elements of spin operators in the ground state manifold are given by $\langle\alpha|\hat{S}_m^a|\alpha'\rangle = -\sigma^a_{\alpha',\alpha}$. Since the ground state of the triangle is given by a spinon hole, it is suggestive to also represent the conduction band in terms of holes $c_{\alpha,m}(\mathbf{x}) \to h^\dagger_{\alpha,m}(\mathbf{x})$, $c^\dagger_{\alpha,m}(\mathbf{x}) \to h_{\alpha,m}(\mathbf{x})$. In the limit of large $J_H$, we thus find a Kondo coupling

$$H_K = \frac{J_K}{N} \sum_{m=1}^{3} (\hat{S}^a)^T h^\dagger_{m,\alpha}(0) (\sigma^a)^T_{\alpha\beta} h_{m,\beta}(0), \quad (4)$$

between the spin and a Fermi sea of holes. Thus, at large $J_H$, the model in Eq. (1) is equivalent to the 3CK problem in the conjugate representation of $SU(N)$, which is equivalent to the 3CK Kondo model, an exactly solvable model (see Appendix A 2). From this mapping, we know that the ground state has an irrational degeneracy of [54–56]

$$g_N = 1 + 2\cos\left(\frac{2\pi}{N+3}\right). \quad (5)$$

Note that $\lim_{N\to\infty} g_N = 3$. We now develop an approximate field theoretical technique which connects the two limits of the phase diagram, Fig. 1.

## IV. LARGE-$N$ TREATMENT

### A. Hubbard-Stratonovich decoupling

Representing the spins using Abrikosov pseudofermions leads to four-fermion interactions, which we decouple using Hubbard-Stratonovich transformation in the leading channels, selected by the large-$N$ limit [see Fig. 2(a) for illustration]:

$$\begin{aligned} S = S_c + \int d\tau \sum_m \Big[ & f^\dagger_{\alpha,m}(\partial_\tau + \lambda_m) f_{\alpha,m} \\ & - \lambda_m q N + \frac{N|V_m|^2}{J_K} + \frac{N|t_m|^2}{J_H} \\ & + (V_m f^\dagger_{\alpha,m} c_{\alpha,m} - t_m f^\dagger_{\alpha,m} f_{\alpha,m+1} + \text{H.c.}) \Big]. \end{aligned} \quad (6)$$

Here, $t_m = |t_m| e^{iA_m}$, $V_m = |V_m| e^{ia_m}$, and the Lagrange multipliers $\lambda_m$ enforce the constraint (for details, see Appendix B).

### B. Mean-field solution

#### 1. *Mean-field Ansätze*

In the limit $N \to \infty$, the bosonic path integrals can be evaluated at the saddle point level for static configurations of the fields. At $T_K = V_m = 0$, Fig. 3(a) demonstrates the stability of homogeneous solutions with $t_m = te^{iA_m}$ and zero or $\pi$ flux $\Phi = \sum_m A_m$ away from half-filling. In the reverse limit $J_H = t_m = 0$, the equality of Kondo couplings at each

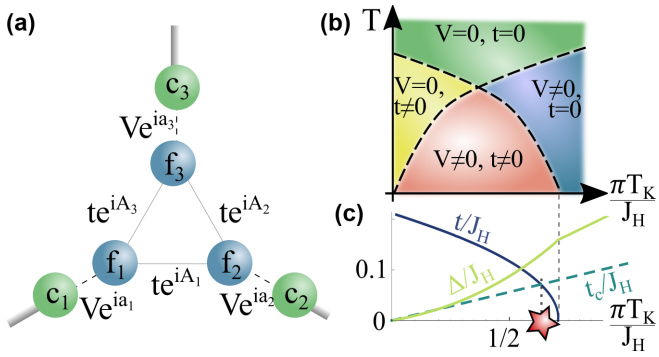


FIG. 2. (a) Pictorial representation of the mean-field Hamiltonian. (b) Schematic mean-field phase diagram. (c) Zero temperature, mean-field behavior of $t$, $\Delta = \pi\rho V^2$ as a function of the Doniach parameter (here, $J_4 = 0.3J_H$, $J_s \sim 0.29J_H$). The position where $t_c$, defined in Eq. (21) below, crosses $t$ defines the confinement-deconfinement quantum phase transition at which phase slips proliferate (red star; here, $N = 4$ and $q = \frac{1}{4}$).

of the three sites implies the same hybridization $|V_m|$ for all $m$. In Read-Newns gauge, the phase of $V_m$ is absorbed into $\lambda_m$, which also takes the same mean-field value at each site. Motivated by this, we concentrate on rotationally symmetric solutions $V_m = V$, $|t_m| = t$, and $\lambda_m = \lambda$, all real, and $q < \frac{1}{3}$. In this case, the spectrum can be found by Fourier transformation, leading to a spinon spectrum $\lambda_h = \lambda - 2t\cos(h + \Phi/3)$, see Fig. 3(b). Here, we introduced the helicity $h = 0, \pm 2\pi/3$ (the crystal momentum of the periodic three-site chain). Using this solution, the fermionic path integral can be taken exactly and leads to a free energy

$$\frac{F}{N} = -T\sum_{\epsilon_n,h} \ln\left[-G_h^{-1}(\epsilon_n)\right]e^{i\epsilon_n\eta} + 3\left(\frac{t^2}{J_H} + \frac{\Delta}{\pi\rho J_K} - \lambda q\right). \tag{7}$$

Here, $G_h^{-1}(\epsilon_n) = i\epsilon_n - \lambda_h + i\Delta sgn(\epsilon_n)$ in the wide bandwidth limit, where $\Delta = \pi\rho V^2$ is the hybridization energy related to $V$ and the density of states $\rho$. The variation of the free energy with respect to the parameters $\Phi$, $\lambda$, $\Delta$, and $t$ leads to a set of mean-field equations of which we discuss the solutions below.

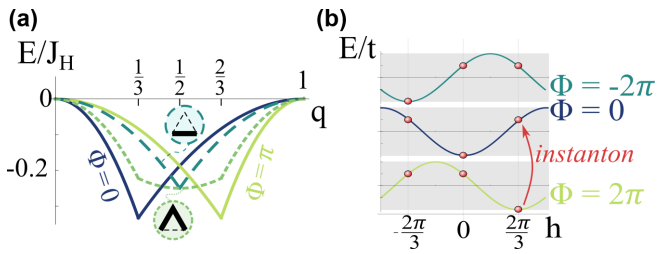


FIG. 3. (a) Ground state energies at $T_K = 0$ as a function of filling $q$, comparing rotationally symmetric solutions (labeled by their flux $\Phi$) with symmetry broken states with one (two) nonzero $t_m$ [graphically labeled by triangles with one (two) thick bonds]. (b) Single particle spectra of spinons at $T_K = 0$ with helicity quantum numbers $h \in \{0, \pm 2\pi/3\}$ for different flux configurations $\Phi = 0, \pm 2\pi$. Instantons map $\Phi \to \Phi \pm 2\pi$ and thereby reshuffle the wave functions but leave the spectrum unaltered.

#### 2. Finite temperature phase diagram

Before presenting details about these equations at zero temperature, we discuss the finite temperature mean-field phase diagram, Fig. 2(b) (a calculation of mean-field transition temperatures is presented in Appendix B 3).

(i) At the highest temperature, the spinons are decoupled, both from each other ($t = 0$) and from their respective conduction band ($V = 0$), so the impurity spins are neither entangled nor screened. This is characterized by decoupled spins showing Curie susceptibility behavior.

(ii) For $T < T_K$ and large $T_K/J_H$, all moments are individually screened (LFL), i.e., $t = 0$, but $V > 0$.

(iii) At smallest $T_K/J_H \ll 1$ and finite temperature, $t > 0$, but $V = 0$; here, a miniature spin-liquid behavior develops. Since the phase shift for all conduction bands is zero, we denote this phase LFL* [21] in Fig. 1(b).

(iv) Finally, the mean-field phase $n$, for which both $V > 0$ and $t > 0$, is the focus of the rest of the paper. We will show that there is a deconfinement transition inside this mean-field phase.

Next, we derive the mean-field transition between these zero temperature phases to map out the mean-field phase diagram.

#### 3. Zero temperature mean-field equations

We now investigate the two zero temperature phases. We readily find that $\Phi = 0$ is a solution to the mean-field equations, and we concentrate on this solution for $q < \frac{1}{2}$. It is convenient to replace the three other variational parameters $(\lambda, \Delta, t)$ by $(\delta_0, \delta_{2\pi/3}, t)$, where $\delta_h = \delta_{-h} = \text{arccot}(\lambda_h/\Delta)$ is the phase shift in the helicity channel $h$. The variation of the free energy with respect to the Lagrange multiplier $\lambda$ enforces a sum rule

$$3\pi q = \delta_0 + 2\delta_{2\pi/3}, \tag{8a}$$

while the variation with respect to $t$ connects the difference $d = \delta_{2\pi/3} - \delta_0$ of phase shifts with the spinon hopping

$$3\pi t = -J_H d. \tag{8b}$$

Note that $t > 0$ implies $d < 0$. The third saddle point equation follows from the variation of the action with respect to $\Delta$. We exploit the previous equation and obtain

$$\left[\frac{\sin(d)}{d}\frac{\pi T_K}{J_H}\right]^3 = \sin\left(\frac{3\pi q + d}{3}\right)\sin^2\left(\frac{3\pi q - 2d}{3}\right). \tag{8c}$$

Note that there is only one variational parameter $d$ in this equation, while $q$ and $\pi T_K/J_H$ are fixed externally. For a graphical solution of Eq. (8c), see Fig. 4. It demonstrates that, for $q = \frac{1}{3}$, a state where both $t \neq 0$ and $V \neq 0$ is never the ground state, while for $q < \frac{1}{3}$, of prime interest in this paper, there is a phase with $t \neq 0$ and $V \neq 0$ which persists to the smallest $T_K/J_H$ and is separated from the LFL by a first-order phase transition (an artifact of the mean-field approach).

### C. Symmetries

Here, we summarize the underlying symmetry breaking using the language of conventional phase transitions. We emphasize, however, that no physical symmetry is broken in

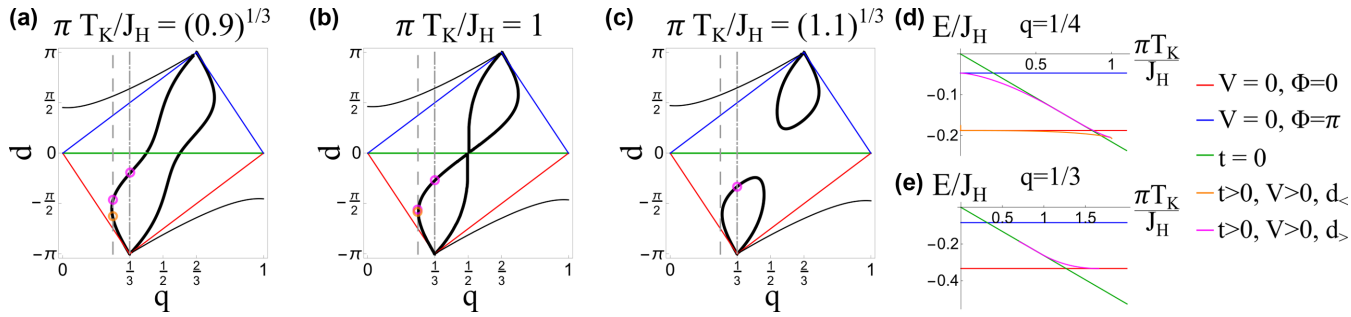


FIG. 4. Graphical illustration of mean-field solutions. (a)–(c) Each point on the black curves corresponds to a solution of Eq. (8c) for a given value of the Doniach parameter $\pi T_K/J_H$. For $q < \frac{1}{2}$ ($q > \frac{1}{2}$), we concentrate on $d < 0$ ($d > 0$) (other solutions are "false vacua" indicated as thin lines). For comparison, we include analogous curves of solutions in the limit $T_K = 0$ [$t > 0, V = 0$ (red) and $t < 0, V = 0$ (blue)] as well as $J_H = 0$ [$t = 0, V > 0$ (green)]. The vertical gray dashed lines indicate the position of $q = \frac{1}{4}, \frac{1}{3}$. For $q = \frac{1}{4}$, there are up to two nontrivial solutions with $-\pi < d < 0$ (orange and pink circles, denoted $d_<$ and $d_>$, respectively), while for $q = \frac{1}{3}$, there is only one nontrivial solution (pink circle) in addition to the solution $d = -\pi$ corresponding to complete Kondo breakdown ($V = 0$). The corresponding mean-field energy is plotted with the same color code in (d) and (e) and compared with the solutions where either $V = 0$ or $t = 0$.

either the 3CK or LFL phase. A parallel discussion in terms the projective symmetry groups (PSGs) is therefore included in Sec. IV E, below.

In the $UV$ ($t = V = 0$), Eq. (6) displays a symmetry $U_f(1)^{\otimes 3} \times U_c(1)^{\otimes 3}$ (i.e., $f_m \to e^{i\phi_m(\tau)} f_m$, $c_m \to e^{i\varphi_m} c_m$), of which $U_f(1)^{\otimes 3}$ is a gauge symmetry. The Kondo effect on each site $m$ ($V_m \neq 0$) breaks the symmetry as $U_f(1)^{\otimes 3} \times U_c(1)^{\otimes 3} \to U_{cf}(1)^{\otimes 3} \equiv G$, fixing $\varphi_m = \phi_m$ for each spin/bath $m$ separately. The three Goldstone modes are eaten by the Lagrange multiplier $\lambda_m$ within the Read-Newns gauge [57]. Most interesting for this paper is the establishment of a spin liquid, in which $|t| > 0$ fixes $\phi_m = \phi + j(m-1)\frac{2\pi}{3}$ with $j \in \{0, 1, 2\} = \mathbb{Z}_3$. Thus, the remaining symmetry $H = U_{cf}(1) \times \mathbb{Z}_3$ is generated by the total phase $\phi$ and the insertion of a total flux of $2\pi j$, i.e., a large gauge transformation which leaves the spectrum unchanged, but rearranges the eigenstates, Fig. 3(b). The symmetry breaking $G \to H$ is apparent within the Landau free energy, which we derived (see Appendix B 4) at $T = 0, V > 0$, and small $\bar{t} = |t_m|/T_K$:

$$\frac{F}{N} = T_K[\alpha \bar{t}^{\,2} - \beta \bar{t}^{\,3} \cos(\Phi) + \gamma \bar{t}^{\,4} + O(\bar{t}^5)], \tag{9}$$

where $\alpha = 3T_K/J_H - \sin(\pi q)/\pi$. The flux $\Phi = \sum_m A_m \in [0, 6\pi)$, but Eq. (9) is $2\pi$ periodic in the total flux, pointing to the emergent $\mathbb{Z}_3$ gauge symmetry of the problem.

### D. Bilinear coupling and ring exchange

The Landau free energy illustrates the first-order nature of the mean-field transition: The cubic term is a consequence of the threefold symmetry of the impurity, and additionally, the microscopic parameters in Eq. (1) imply $\gamma < 0$ near the transition, reinforcing the first-order behavior. A negative quartic term is typical in the large-$N$ treatments and can be cured by inclusion of a biquadratic interaction [22]:

$$H_4 = -\frac{\pi^3 J_4}{2N^3} \sum_m \left(\hat{S}^a_m \hat{S}^a_{m+1}\right)^2, \tag{10}$$

leading to $\gamma = 3[J_4 \sin(\pi q)^4/T_K - \sin(3\pi q)]/(2\pi)$. The first-order jump is further weakened by the addition of a totally symmetric ring exchange:

$$H_3 = -\pi^2 \frac{J_s}{N} d_{abc} \hat{S}^a_1 \hat{S}^b_2 \hat{S}^c_3, \tag{11}$$

so that microscopically $\beta = [\sin(2\pi q) - J_s \sin(\pi q)^3/T_K]/\pi$ after integration of fermions. A similar integration is the origin of the relation $\mathcal{O}_s \sim \cos(\Phi)$ presented in Eq. (2).

Ring exchange terms can be employed to physically access the emergent gauge flux $\Phi$. An adiabatic flux insertion can be achieved by adiabatically tuning $\theta(t)$ in

$$\Delta H(t) = -\frac{J}{N}[d_{abc} \cos\theta(t) + f_{abc} \sin\theta(t)] \hat{S}^a_1 \hat{S}^b_2 \hat{S}^c_3,$$

where $d_{abc}$ and $f_{abc}$ are symmetric and antisymmetric structure factors of $SU(N)$. A mean-field decoupling of $H + \Delta H$ leads to $\Delta F \propto -J \cos(\Phi - \theta)$.

### E. A study of PSGs

We now return to the emergent gauge invariance in the problem and employ the method of PSGs, introduced [58] to categorize gapless spin liquid states which do not break any microscopic (e.g., crystalline) symmetries. To recapitulate the procedure:

(i) Consider a mean-field tight-binding model of spinons $f_{\alpha,m}$, in our case Eq. (6). Because spinons carry an emergent gauge charge, mean-field tight-binding models which can be transformed into each other by means of a gauge transformation are equivalent.

(ii) The group of microscopic symmetry operations followed by a gauge transformation which leave the tight-binding model invariant form the PSG of the model.

(iii) The subgroup of gauge transformations which leave the tight-binding Hamiltonian invariant form the invariant gauge group (IGG).

(iv) The actual symmetry group (SG) of the model is thus SG = PSG/IGG. Hence, the PSG can be seen as an extension of the SG.

The IGG also places constraints on Wilson loop operators $P_C$ [2], which are products of Peierls gauge fields along closed contours on links of the lattice ($P_C = \prod_{m=1}^3 e^{iA_m}$ in our simple three-site lattice). Wilson loops are a particularly useful def-

inition for gapless topological quantum states when standard signatures (such as a degenerate ground state manifold) are less obvious.

As mentioned, in our case, the infrared gauge transformations are $f_{\alpha,m} \to e^{i\phi_m} f_{\alpha,m}$, $c_{\alpha,m} \to e^{i\phi_m} c_{\alpha,m}$, and $A_m \to A_m + \phi_m - \phi_{m+1}$ and imply an IGG which is $U(1)$. The crystalline symmetries group of the triangle is generated by 120° rotations $R$, $R^3 = 1$, and an involutory mirror operation $M = M^{-1}$ exchanging sites $m = 1 \leftrightarrow m = 2$. They do not commute; instead, $MRMR = 1$. We may then proceed with the analysis of the PSG assuming deconfining gauge fields. To projectively represent the rotation, we perform a gauge transformation $f_m \to G_R(m) f_m$, $c_m \to G_R(m) c_m$ with $G_R(m) = e^{iA_m}$ after application of the crystalline symmetry operation. Analogously, the mirror exchanging sites $1 \leftrightarrow 2$ are projectively represented by employing $G_M(m) = e^{i(A_3 - A_2)\delta_{m,3}}$. Since we assume time-reversal symmetry, there is a gauge in which all hopping matrix elements are real, i.e., $A_m \in \{0, \pi\}$. Then the algebra of projective symmetry operations is $(G_R R)^3 = e^{i\Phi} = \pm 1$, $(G_M M)^2 = 1$, $(G_M M)(G_R R)(G_M M)(G_R R) = 1$. Thus, the two mean-field states associated with $\Phi = 0, \pi$ in Fig. 3(a) are categorized by different algebraic PSGs. On the mean-field level, these two states are separated by multiple symmetry broken states—this is reminiscent of the transition between 2D quantum phases with different PSGs coupled to fermionic matter [59].

## V. FLUCTUATIONS AND GAUGE FIELDS

In the previous section, we discussed the mean-field solution to Eq. (1), which is valid at $N = \infty$. Here, we consider fluctuation corrections beyond this limit.

### A. Dynamics of low-energy excitations

The bosonic low-energy excitations in the model are the phases $A_m$, whose action may be derived microscopically by a lengthy but straightforward integration of fermionic degrees of freedom, see Appendix C, leading to $S(A_m) = S_{\rm diss} + S_{\rm Maxwell}$:

$$S_{\rm diss} = \int \frac{d\omega}{2\pi} \frac{\eta}{4\pi} \Phi(\omega)\Phi(-\omega)|\omega|, \tag{12a}$$

$$S_{\rm Maxwell} = \int d\tau \sum_m \frac{\epsilon}{2} \dot{A}_m^2, \tag{12b}$$

where

$$\eta \simeq 3N \frac{t^2}{T_{\rm K}^2} \sin^2(\pi q), \quad [\text{for } t \ll T_{\rm K} \cos(\pi q)], \tag{13a}$$

$$\epsilon = \frac{2N}{9J_{\rm H}} \left[ 1 + \frac{J_{\rm H} \sin(\delta_{2\pi/3})^2}{2\pi\Delta} \right] (1 + 2\rho\Delta). \tag{13b}$$

Here, we presented the microscopic expression for the low-energy ($|\omega| \ll T_{\rm K}$) dissipative dynamics of $\Phi$ in the limit $t \ll T_{\rm K}$ [near the QCP, see Fig. 2(c)]. For a more comprehensive expression, see Eq. (C16) of the Appendix.

Before discussing the features of this emergent gauge theory, we analyze the fluctuations using the more conventional language of Goldstone bosons.

### B. Goldstone bosons

When $t/t_{\rm K} > 0$, two combinations of $A$ phases, parametrized by $A_m = -2\vec{x} \cdot \hat{e}_m/3$, where $\hat{e}_{1,2} = (\pm\sqrt{3}, 1)/2$, $\hat{e}_3 = (0, -1)$, and $\vec{x} = (x_1, x_2)$, are zero modes of the free energy Eq. (9) and parametrize the manifold of Goldstone bosons (see Sec. IV C):

$$\frac{G}{H} = \frac{U(1) \times U(1) \times U(1)}{U(1) \times \mathbb{Z}_3}. \tag{14}$$

In contrast, the third linear combination of phases $\Phi = \sum_m A_m$ is gapped. For $J_{\rm H} \gg T_{\rm K}$, the two brackets entering $\epsilon$ in Eq. (13b) are approximately one, so we omit them for simplicity. The effective action of Goldstone bosons is thus

$$S_{\rm Goldstone}(\vec{x}) = \int d\tau \frac{m_x \dot{\vec{x}}^2}{2}, \tag{15}$$

where $m_x = 8N/(27J_{\rm H})$. This action describes a free particle with position $\vec{x}$ and mass $m_x$ living on the flat, yet compact manifold in Eq. (14). The ground state is an $\vec{x}$-independent wave function and, due to the compactness of $G/H$, detached from the first excited state at energy $\sim 1/m_x$.

As a consequence, despite the mean-field value $t > 0$, intersite Green's functions $\langle c_m^\dagger c_{m+1} \rangle \sim \langle e^{iA_m} \rangle$ vanish upon integration of Goldstone modes. Therefore, the absence of charge transfer between different leads is ensured by the fluctuations beyond the $N \to \infty$ limit. Equivalently, this can be interpreted as a consequence of gauge symmetry which impedes charge fluctuations on the impurity sites.

### C. Confinement-deconfinement transition

So far, we incorporated leading terms in a $1/N$ series. Now we address processes with Boltzmann weight $\Gamma \sim e^{-N}$ (instantons). Naively, these are strongly suppressed, yet we demonstrate a proliferation of instantons at sufficiently large $T_{\rm K}/J_{\rm H}$. Instantons in gauge theories are nontrivial gauge field configurations which are bound to be a pure gauge at infinity. In the present case, these are phase slips, i.e., configurations of the field $\Phi(\tau)$ such that $\Phi(\infty) - \Phi(-\infty) = \pm 2\pi$, and we estimate their bare tunneling action $\Gamma \sim e^{-N\bar{t}}$ for $\beta \ll \bar{t}$ in Appendix C 3.

Considering Eq. (6) with static fields $t, V$, we can artificially introduce [29] an additional Hilbert space associated to $\Phi = 0, 2\pi, 4\pi$. To manifestly illustrate the effect of phase slips, we define $\omega = e^{i2\pi/3}$ and the following two matrices in the space of groundstate manifold:

$$\sigma_\Phi = \begin{pmatrix} 1 & & \\ & \omega & \\ & & \omega^2 \end{pmatrix}, \quad \tau_\Phi = \begin{pmatrix} 0 & 0 & 1 \\ 1 & 0 & 0 \\ 0 & 1 & 0 \end{pmatrix}. \tag{16}$$

Here, $\tau_\Phi$ are clock matrices $\sigma_\Phi \tau_\Phi = \omega \tau_\Phi \sigma_\Phi$, $\tau_\Phi^3 = 1$. The phase slips accompanying spinon hoppings are considered by replacement $t \to t\sigma_\Phi$.

The infinite resummation of phase slips of the latter in the partition sum leads to an effective Hamiltonian derived in Appendix D 2:

$$H_{\rm eff} = \left[ H_c + \sum_m \lambda (f_{\alpha,m}^\dagger f_{\alpha,m} - Q) \right] 1_\Phi - \Gamma \left( \tau_\Phi + \tau_\Phi^{-1} \right) + \sum_m (V f_{\alpha,m}^\dagger c_{\alpha,m} 1_\Phi - t f_{\alpha,m}^\dagger f_{\alpha,m+1} \sigma_\Phi + \text{H.c.}). \tag{17}$$

In the formulation of Eq. (17), two limiting cases become apparent. First, $\Gamma/t \to 0$, representing the 3CK phase. Second, perturbation about $\Gamma/t \to \infty$ demonstrates that $t$ is renormalization group irrelevant, and the LFL is restored.

To study the transition between these two limiting phases, we consider the helical (i.e., Fourier transformed) basis $\tilde{f}_{\alpha,h} = \sum_m e^{-ihm} f_{\alpha,m}/\sqrt{3}$. A phase slip $t \to \omega t$ is equivalent to the instantaneous jump of the spinon energy $(t, -2t, t) \to (t, t, -2t)$ for $h = (-2\pi/3, 0, 2\pi/3)$, Fig. 3(b). Due to hybridization with conduction electrons, a phase slip triggers an Anderson orthogonality catastrophe and thereby logarithmic attraction of opposite phase slips, $\Delta\tau$ apart, with an effective action

$$S_{\text{slips}} = \kappa \ln|\Delta\tau|. \tag{18}$$

Here,

$$\kappa = \frac{2N}{\pi^2}\left[\arctan\left(\frac{3t\Delta}{\Delta^2+\lambda^2}\right)\right]^2, \tag{19}$$

is the stiffness of interaction as determined by the perturbative inclusion of a single pair of opposite phase slips at distance $\Delta\tau$ in the fermionic partition sum, see Appendix D 1. Integration over $\Delta\tau$ leads to the free energy

$$F = -\ln(g_N)T - \mathcal{C}\left(\frac{\Gamma^2}{\lambda}\right)\left(\frac{T}{\lambda}\right)^{\kappa-1}, \tag{20}$$

where we included the effect of the ground state degeneracy $g_N$, Eq. (5), and $\mathcal{C}$ is a constant. This signals a quantum phase transition when the phase slips overpower the first term at $\kappa = 2$, corresponding to, Fig. 2(c),

$$t_c \sim \frac{T_{\text{K}}\sin(\pi q)}{\sqrt{N}}. \tag{21}$$

The residual entropy at the QCP is enhanced to $S = \ln(g_N) + \mathcal{C}\Gamma^2/\lambda^2 + \mathcal{O}(\Gamma^4/\lambda^4)$ by the instanton contribution, in consistency with the $g$ theorem [60]. The present model of logarithmically interacting particles on a ring of circumference $1/T$ can be cast into renormalization group language [61]: $\Gamma$ renormalizes to infinity (zero) for $t < t_c$ ($t_c < t$). However, contrary to the Berezinskii-Kosterlitz-Thouless transition, the stiffness $\kappa$ does not flow.

So far, the deconfinement transition was studied by first locking $\Phi$ into one of the minima of Eq. (9) and subsequent perturbative inclusion of phase slips. The same transition may also be studied in a dual language [approaching the red star of Fig. 1(b) from the right]. In this case, $\Phi$ is free to fluctuate, and $\beta \ll 1$ is considered as a perturbation. From this perspective, the 3CK (FL) is the phase where $\beta$ is relevant (irrelevant). Crucially, near the transition, the dynamics of the $\Phi$ field is overdamped due to the interaction with the conduction bath, see Eqs. (12a) and (13a). The problem of dissipative tunneling, i.e., $S = S_{\text{diss}} - \int d\tau N T_{\text{K}} \beta \cos[\Phi(\tau)]$, for small $\beta$ yields a scaling equation

$$\frac{d\beta}{d\ell} = \left(1 - \frac{1}{\eta}\right)\beta, \tag{22}$$

where $d\ell = -\log D$ in terms of the running cutoff [62,63], while the nonanalytical nature of the kinetic (i.e., damping) term is believed to prevent a renormalization of $\eta$ to all orders [61]. The condition $\eta > 1$ for relevant $\beta$ is parametrically equivalent to $t > t_c$, with $t_c$ given in Eq. (21). In the dual language, it is manifest that Goldstone bosons $\vec{x}$ do not affect the nature or position of the transition because they are by construction perpendicular to $\Phi$.

### D. 3CK phase in fractionalized language

Before concluding, we briefly reiterate the connection to the 3CK problem for $T_{\text{K}} \ll J_{\text{H}}$ in fractionalization language.

In this limit, it is convenient to evaluate Eq. (17) in a gauge in which $t$ is real and positive. Since $\Gamma$ is irrelevant in this phase, $\sigma_\Phi$ is conserved. We project on the ground state (zero helicity $h = 0$) of the $f$ electrons [Fig. 3(a)] and obtain the effective Kondo Lagrangian

$$\mathcal{L}_{\text{Kondo}} = \sum_m \left[(\tilde{f}^\dagger_{\alpha,0} V_m c_{\alpha,m} + \text{c.c.}) + \frac{|V_m|^2}{J_{\text{K}}}\right], \tag{23}$$

with constraint $\tilde{f}^\dagger_{\alpha,0}\tilde{f}_{\alpha,0} = 3Q$. As anticipated previously, three channels of conduction electrons are screening a single spin, and 3CK physics is expected. The soft modes associated with rotations of $|V_m|$ are gapped for $T_{\text{K}}/J_{\text{H}} > 0$ enforcing $V_m = Ve^{ia_m}$. Based on this observation, we conjecture that the physics discussed here for the 3CK phases of our Kondo triangle applies more generally to single-impurity 3CK systems and more generic overscreened Kondo problems.

## VI. CONCLUSIONS

We conclude with a discussion of multichannel Kondo phases as representatives of topological order and of possible experimental and numerical implications of our findings.

### A. Signatures of topological order

While there is no magnetic ordering in any of the phases, the symmetric ring exchange operator $\mathcal{O}_s = d_{abc}\hat{S}^a_1\hat{S}^b_2\hat{S}^c_3$ displays order in the 3CK phase. The ordering of such a composite operator is like *order by disorder* [64–66] or *vestigial order* [67] phenomena and would suggest a characterization of the 3CK phase in terms of a generalization of spontaneous symmetry breaking.

However, we here propose a different interpretation and put forward the hypothesis that multichannel Kondo states display a form of topological order which is like the quantum order in gapless QSLs. For the 3CK phase scrutinized here, the evidence is as follows.

First, as mentioned, the 3CK phase does not break any of the physical symmetries in the original model in Eq. (1), even when the $\mathcal{O}_s$ orders. This invalidates any interpretation of the 3CK in terms of spontaneous symmetry breaking—instead, we have presented a categorization using the PSG. Second, regarded as an operator in the gauge theory, $\mathcal{O}_s \sim \text{Re}(e^{i\sum_m A_m})$ is a miniature Wilson loop. In macroscopically extended systems, this would be taken as a clear signal of deconfinement. Third, the order of $\mathcal{O}_s$ is destroyed by the proliferation, or condensation, of monopoles in the FL, which on the other

hand are gapped in the 3CK phase. This is reminiscent of the situation in $QED_3$, while the expulsion of topological defects is generically a defining characteristic of topological states [68]. Finally, the 3CK displays an irrational ground state degeneracy indicating gapless anyonic excitations, another striking signature of topological order.

At the same time, multichannel Kondo states are often unstable toward anisotropic coupling to the leads (see, e.g., Refs. [69,70] for exceptions). As mentioned, while the 3CK phase studied here is stable for unequal $J_H$, it is unstable if $J_K$ are unequal. This suggests the interpretation of the 3CK phase as a symmetry-protected topological state of matter or as a deconfined quantum critical fixed point.

### B. Relevance for experiment and numerics

Beyond its purpose as an analytically tractable toy model, our investigations are relevant to the simplest cluster-dynamical mean-field theory [71,72] approaches to Hubbard models on triangular lattices, which have enjoyed increased interest in recent times [73,74]. The $SU(4)$ case studied here might be of importance for twisted bilayer graphene [75,76] with approximate valley symmetry. Emergent $SU(4)$ symmetric spin interactions [77–79] were also recently predicted in spin-orbit coupled transition metal trihalides with low-lying $J_{\text{eff}} = \frac{3}{2}$ quartets [80]. Here, $SU(N)$ symmetric interactions of strongly correlated fermions with large flavor number $N$ have moreover been realized in cold atomic quantum emulators [81,82]. We conclude with the prospect of directly probing the presented theory in quantum dot experiments: Recent advance on $SU(4)$ impurities [83], triangle [84], and 3CK [85] physics may allow us to artificially fabricate the setup, Fig. 1(a), and thereby conduct an experimental study of the deconfinement transition.


## ACKNOWLEDGMENTS

The authors appreciate discussions with P. Chandra, W. Metzner, Th. Schäfer, and E. Sela. E.J.K. was supported by Department of Energy Basic Energy Sciences Grant No. DE-FG02- 99ER45790. P. C. and Y. K. were support by National Science Foundation Grant No. DMR-1830707.


## APPENDIX A: MAPPING TO A 3CK PROBLEM

This section is devoted to the mapping of the frustrated triangle to a 3CK problem and contains details for Sec. III of the main text. This mapping is possible for the sequence of models with $SU(4), SU(7), SU(10)\ldots$ (i.e., $N \in 3\mathbb{N}+1$) symmetry at filling $q = \frac{1}{4}, \frac{2}{7}, \frac{3}{10}, \ldots$ [i.e., $Q = (N-1)/3$] and is valid when $J_H$ is the largest scale.

### 1. Solution of the triangle alone

We represent a given spin configuration with fixed particle number per site $Q = (N-1)/3$ by

$$|\alpha_1 \ldots \alpha_Q; \alpha_{Q+1} \ldots \alpha_{2Q}; \alpha_{2Q+1} \ldots \alpha_{3Q}\rangle = f^\dagger_{1,\alpha_1} \cdots f^\dagger_{1,\alpha_Q} f^\dagger_{2,\alpha_{Q+1}} \cdots f^\dagger_{2,\alpha_{2Q}} f^\dagger_{3,\alpha_{2Q+1}} \cdots f^\dagger_{3,\alpha_{3Q}} |\underline{0}\rangle . \tag{A1}$$

In this manifold, the spin is faithfully represented as

$$\hat{S}^a_m = f^\dagger_{\alpha,m} \sigma^a_{\alpha\beta} f_{m,\beta}. \tag{A2}$$

We next act on Eq. (A1) with the Hamiltonian

$$H_H = \frac{J_H}{N} \sum_{m=1}^{3} \left( f^\dagger_{m,\alpha} f_{m,\beta} f^\dagger_{m+1,\beta} f_{m+1,\alpha} - \frac{f^\dagger_{m,\alpha} f_{m,\alpha} f^\dagger_{m+1,\beta} f_{m+1,\beta}}{N} \right). \tag{A3}$$

The last term yields a mere shift of energy $3Q^2 J_H/N^2$ for any of the states Eq. (A1), so we omit it. The action of the first term is the sum of permutations of two spin indices from adjacent sites:

$$\begin{aligned} H_H &|\alpha_1 \ldots \alpha_Q; \alpha_{Q+1} \ldots \alpha_{2Q}; \alpha_{2Q+1} \ldots \alpha_{(N-1)}\rangle \\ &= \frac{J_H}{N} \{ |\alpha_{Q+1} \ldots \alpha_Q; \alpha_1 \ldots \alpha_{2Q}; \alpha_{2Q+1} \ldots \alpha_{(N-1)}\rangle \\ &\quad + |\alpha_1, \alpha_{Q+1} \ldots \alpha_Q; \alpha_2, \alpha_{Q+2} \ldots \alpha_{2Q}; \alpha_{2Q+1} \ldots \alpha_{(N-1)}\rangle + (\text{similar perm. between sites 1,2}) \\ &\quad + |\alpha_1 \ldots \alpha_Q; \alpha_{2Q+1} \ldots \alpha_{2Q}; \alpha_{Q+1} \ldots \alpha_{(N-1)}\rangle + (\text{similar perm. between sites 2,3}) \\ &\quad + |\alpha_{2Q+1} \ldots \alpha_Q; \alpha_{Q+1} \ldots \alpha_{2Q}; \alpha_1 \ldots \alpha_{(N-1)}\rangle + (\text{similar perm. between sites 3,1})\}. \end{aligned} \tag{A4}$$

Therefore, eigenstates $|\psi\rangle$ are obtained by sums over symmetric/antisymmetric permutations (Einstein summation convention is employed):

$$|\psi\rangle = t_{\alpha_1,\ldots,\alpha_Q;\alpha_{Q+1}\ldots\alpha_{2Q};\alpha_{2Q+1}+\alpha_{3Q}} |\alpha_1, \ldots, \alpha_Q, \alpha_{Q+1} \ldots \alpha_{2Q}, \alpha_{2Q+1} + \alpha_{3Q}\rangle . \tag{A5}$$

We concentrate on the ground state, where the tensor has the following antisymmetry properties:

$$t_{\alpha_1,\alpha_2\ldots,\alpha_Q;\alpha_{Q+1}\ldots\alpha_{2Q};\alpha_{2Q+1}+\alpha_{3Q}} = -\, t_{\alpha_2,\alpha_1\ldots,\alpha_Q;\alpha_{Q+1}\ldots\alpha_{2Q};\alpha_{2Q+1}+\alpha_{3Q}} \quad \text{(Fermi-Dirac statistics within a given site)}, \tag{A6}$$

$$t_{\alpha_1,\alpha_2\ldots,\alpha_Q;\alpha_{Q+1}\ldots\alpha_{2Q};\alpha_{2Q+1}+\alpha_{3Q}} = -\, t_{\alpha_{Q+1},\ldots,\alpha_Q;\alpha_1\ldots\alpha_{2Q};\alpha_{2Q+1}+\alpha_{3Q}} \quad (H_H \text{ favors pairwise antisymmetry across sites}). \tag{A7}$$

To get the total number of states, we start by overcounting allowed possibilities. There are $N$ options to place $\alpha_1$, $N-1$ to place $\alpha_2$, etc., leading to

$$\frac{N!}{(N-3Q)!}, \tag{A8}$$

states. However, we overcounted $3Q!$ different permutations, so the actual number of states is just

$$\binom{N}{3Q} = \binom{N}{N-1} = N. \tag{A9}$$

Thus, the following completely antisymmetrized eigenstates are the ground state of the triangle at filling $Q$:

$$|\alpha_N\rangle = \frac{\epsilon_{\alpha_1\ldots\alpha_N}}{\sqrt{\mathcal{N}}} |\alpha_1\ldots\alpha_Q;\alpha_{Q+1}\ldots\alpha_{2Q};\alpha_{2Q+1}\ldots\alpha_{(N-1)}\rangle\,. \tag{A10}$$

Here and in the following, we label numerical normalization factors by $\mathcal{N}$. This concludes the derivation of Eq. (3). There, we use the notation

$$|\text{singlet}, m=1\rangle = \frac{\epsilon_{\alpha_1\ldots\alpha_N}}{\sqrt{\mathcal{N}}} |\alpha_1\ldots\alpha_{Q+1};\alpha_{Q+2}\ldots\alpha_{2Q+1};\alpha_{2Q+2}\ldots\alpha_N\rangle\,, \tag{A11}$$

and analogously for $m=2,3$.

### 2. Effective low-energy Hamiltonian

As a next step, we project the Kondo-triangle Hamiltonian onto the ground state manifold spanned by the $N$ states Eq. (A10). We begin by determining the spin representation within the manifold of states Eq. (A10):

$$\begin{aligned}\langle\alpha_N|\hat{S}^a_m|\alpha'_N\rangle &= \frac{\sigma^a_{\beta\beta'}\epsilon_{\alpha_1\ldots\alpha_N}\epsilon_{\alpha'_1\ldots\alpha'_N}}{\mathcal{N}} \langle\alpha_1\ldots\alpha_Q;\alpha_{Q+1}\ldots\alpha_{2Q};\alpha_{2Q+1}\ldots\alpha_{N-1}| \underbrace{f^\dagger_{m,\beta}f_{m,\beta'}}_{\delta_{\beta\beta'}-f_{m,\beta'}f^\dagger_{m,\beta}} |\alpha'_1\ldots\alpha_{Q'};\alpha'_{Q+1}\ldots\alpha'_{2Q};\alpha'_{2Q+1}\ldots\alpha'_{(N-1)}\rangle \\ &= -\tilde{\mathcal{N}}\sigma^a_{\alpha'_N\alpha_N}.\end{aligned} \tag{A12}$$

This result immediately follows from the consideration that all spin quantum numbers except $\alpha_N(\alpha'_N)$ have been used in the ket (bra). Thus, the index of the creation operator $\beta=\alpha'_N$ ($\beta'=\alpha_N$) unless $\beta=\beta'$. We further used $\mathrm{tr}(\sigma^a)=0$. Instead of explicitly calculating the positive proportionality constant, we show that $\tilde{\mathcal{N}}=1$ by

$$\begin{aligned}\sum_{N,N'} \left|\langle\alpha_N|\hat{S}^a_m|\alpha'_N\rangle\right|^2 &= \mathrm{tr}[(\sigma^a)^2] \\ &= \tilde{\mathcal{N}}^2\mathrm{tr}[\{(\sigma^a)^T\}^2].\end{aligned} \tag{A13}$$

Here, the first equality follows from the completeness of $\{|\alpha_N\rangle\}$ and the second equality from the evaluation of the matrix element. Therefore, the effective Hamiltonian has the form

$$H_{\text{eff}} = H_c - \frac{J_\text{K}}{N}\sum_{m=1}^{3}(\hat{S}^a)^T c^\dagger_m \sigma^a c_m. \tag{A14}$$

As a final step, we reverse particle and hole operators $c_m \to h^\dagger_m$, $c^\dagger_m \to h_m$, then

$$H_{\text{eff}} = H_c + \frac{J_\text{K}}{N}\sum_{m=1}^{3}(\hat{S}^a)^T h^\dagger_m (\sigma^a)^T h_m. \tag{A15}$$

This is the origin of Eq. (4) in the main text. To see that Eq. (4), in which spin operators are transposed, is equivalent to the standard 3CK model

$$H_{\text{3CK}} = H_c + \frac{J_\text{K}}{N}\sum_{m=1}^{3}\hat{S}^a h^\dagger_m \sigma^a h_m, \tag{A16}$$

it is sufficient to realize that the $SU(N)$-invariant interaction can be reexpressed using the Fierz identity

$$(\sigma^a)_{\alpha\beta}(\sigma^a)_{\gamma\delta} = \delta_{\alpha\delta}\delta_{\beta\gamma} - \frac{1}{N}\delta_{\alpha\beta}\delta_{\gamma\delta}, \tag{A17}$$

which is invariant under simultaneous transposition operation $(\alpha,\gamma)\leftrightarrow(\beta,\delta)$.

### 3. Robustness against inhomogeneity

At strong coupling, the triangle is robust against moderate inhomogeneities in $J_\text{H}$, as can be seen by the following evaluation of matrix elements of $\delta H = \delta J_\text{H}\hat{S}^a_1\hat{S}^a_2$:

$$\begin{aligned}\langle\alpha_N|\delta H|\alpha'_N\rangle &= \delta J_\text{H}\sum_{\tilde{\alpha}_N}\langle\alpha_N|\hat{S}^a_1|\tilde{\alpha}_N\rangle\,\langle\tilde{\alpha}_N|\hat{S}^a_2|\alpha'_N\rangle \\ &= \tilde{\mathcal{N}}^2\sum_a\sum_{\tilde{\alpha}_N}(\sigma^a)_{\alpha'_N\tilde{\alpha}_N}(\sigma^a)_{\tilde{\alpha}_N\alpha_N} \propto \delta_{\alpha'_N\alpha_N}.\end{aligned} \tag{A18}$$

Thus, inhomogeneities projected to the ground state manifold are proportional to the unit matrix and do not lift the degeneracy of states $|\alpha_N\rangle$.

## APPENDIX B: IMPURITY PARTITION SUM, STATIC EVALUATION

In this section, we present technical details on the evaluation of the partition sum. Throughout this paper, we consider the partition sum (and thus, free energy and effective action) of the impurity alone. This is defined as $\mathcal{Z}_{\text{impurity}} = \mathcal{Z}_{\text{total}}/\mathcal{Z}_{\text{no impurity}}$, where $Z_{\text{total}}$ is given by

$$\mathcal{Z}_{\text{total}} = \prod_{m=1}^{3} \int_0^\infty \mathcal{D}V_m V_m \int_{-i\infty}^{i\infty} \mathcal{D}\lambda_m \int_{\mathbb{C}^2} \mathcal{D}(t_m, t_m^*) \times \int \mathcal{D}(c_m, f_m) e^{-S(V_m,\lambda_m,t_m,c_m,f_m)}. \tag{B1}$$

Note that we employ Read-Newns gauge ($V_m > 0$) throughout this section. The partition sum $\mathcal{Z}_{\text{no impurity}}$ is the same partition sum of the three wires but without any Kondo impurities.

### 1. Diagonalization of spinon Hamiltonian

The spinon Hamiltonian, see also Eq. (6) of the main text, has the form

$$H_t = -t f^\dagger \begin{pmatrix} 0 & e^{iA_1} & e^{-iA_3} \\ e^{-iA_1} & 0 & e^{iA_2} \\ e^{iA_3} & e^{-iA_2} & 0 \end{pmatrix} f, \tag{B2}$$

where we use the three-component notation $f = (f_1, f_2, f_3)$, and similarly for $c(\mathbf{x}) = [c_1(\mathbf{x}), c_2(\mathbf{x}), c_3(\mathbf{x})]$ on each site of the wires. We rotate $f = U\tilde{f}$ and $c = U\tilde{c}$ electrons by $U = \text{diag}[e^{i(A_1-\Phi/3)}, 1, e^{-i(A_2-\Phi/3)}]$, leading to

$$H_t = -t\tilde{f}^\dagger \begin{pmatrix} 0 & e^{i\Phi/3} & e^{-i\Phi/3} \\ e^{-i\Phi/3} & 0 & e^{i\Phi/3} \\ e^{i\Phi/3} & e^{-i\Phi/3} & 0 \end{pmatrix} \tilde{f}. \tag{B3}$$

This rotation appears at the expense of a vector potential

$$(c^\dagger, f^\dagger)\partial_\tau (c, f)^T = (\tilde{c}^\dagger, \tilde{f}^\dagger)(\partial_\tau + i\mathcal{A})(\tilde{c}, \tilde{f})^T, \tag{B4}$$

where

$$\mathcal{A} = -iU^\dagger \partial_\tau U = \text{diag}\left[\dot{A}_1 - \frac{\dot{\Phi}}{3}, 0, -\left(\dot{A}_2 - \frac{\dot{\Phi}}{3}\right)\right]. \tag{B5}$$

It is furthermore useful to expand $\tilde{f}, \tilde{c}$ in eigenstates with instantaneous energy $\epsilon_k = -2t\cos[k + \Phi(\tau)/3]$:

$$|\psi_k\rangle = \frac{1}{\sqrt{3}} \begin{pmatrix} e^{-ik} \\ 1 \\ e^{ik} \end{pmatrix}, \quad k = 0, \pm\frac{2\pi}{3}. \tag{B6}$$

In this basis, the Berry connection is $\mathcal{A}_{k'k} = [(\dot{A}_1 - \dot{\Phi}/3)e^{i(k'-k)} - (\dot{A}_2 - \dot{\Phi}/3)e^{-i(k'-k)}]/3$. In summary, the total Lagrangian under consideration is [we employ the notation $D_\tau = \partial_\tau + i\mathcal{A}$ and $\lambda_k = \lambda + \epsilon_k(\Phi)$]

$$\mathcal{L} = \sum_{k,k'} \begin{bmatrix} \cdots & c^\dagger_{\alpha,k}(\mathbf{p}) & \cdots & f^\dagger_{\alpha,k} \end{bmatrix} \left[\begin{array}{c|c} (D_\tau)_{k,k'} + \epsilon(\mathbf{p})\delta_{\mathbf{p},\mathbf{p}'}\delta_{kk'} & V\delta_{kk'} \\ \hline V\delta_{kk'} & (D_\tau)_{k,k'} + \lambda_k\delta_{kk'} \end{array}\right] \begin{bmatrix} \vdots \\ c_{\alpha,k'}(\mathbf{p}') \\ \vdots \\ f_{\alpha,k'} \end{bmatrix} + 3\left(N\frac{t^2}{J_{\text{K}}} + N\frac{V^2}{J_{\text{K}}} - \lambda q N\right). \tag{B7}$$

### 2. Static fields and mean-field solution

We begin by studying the mean-field solution. At this level, we consider all bosonic fields $V > 0, t > 0, \Phi = \sum_m A_m$ as constant variational parameters, and $\mathcal{A} = 0$. The fermionic integral yields Eq. (7). The mean-field equations involve the following two integrals:

$$n_F \equiv I_1\left(\frac{\lambda}{\Delta}\right) = T\sum_n \frac{e^{i\epsilon_n\eta}}{i\epsilon_n - \lambda + i\Delta s\left(\frac{\epsilon_n}{D}\right)} \simeq \text{arccot}\frac{\left(\frac{\lambda}{\Delta}\right)}{\pi} =: \frac{\delta\left(\frac{\lambda}{\Delta}\right)}{\pi}, \tag{B8a}$$

$$I_2(\lambda + i\Delta) = T\sum_n \frac{is\left(\frac{\epsilon_n}{D}\right)e^{i\epsilon_n\eta}}{i\epsilon_n - \lambda + i\Delta s\left(\frac{\epsilon_n}{D}\right)} \simeq -\frac{\ln(|\lambda + i\Delta|\eta) + \gamma_{\text{EM}}}{\pi}. \tag{B8b}$$

Here, $\gamma_{\text{EM}}$ is the Euler Mascheroni constant {with our regularization scheme $T_{\text{K}} = \exp[-1/(\rho J_K) - \gamma_{\text{EM}}]/\eta$} and $\simeq$ implies a zero temperature calculation. Note that $\delta$ becomes a step function (from $\pi$ down to 0) as $\Delta \to 0$.

Having established these prerequisites, we are now in the position to impose the mean-field equations

$$\frac{1}{N}\frac{\partial F}{\partial \lambda} = \sum_k \left[I_1\left(\frac{\lambda_k}{\Delta}\right) - q\right] \stackrel{!}{=} 0, \tag{B9a}$$

$$\frac{1}{N}\frac{\partial F}{\partial \Delta} = \sum_k \left[-I_2\left(\frac{\lambda_k}{\Delta}\right) + \frac{1}{\pi\rho J_{\text{K}}}\right] \stackrel{!}{=} 0, \tag{B9b}$$

$$\frac{1}{N}\frac{\partial F}{\partial t} = \sum_k \left[\frac{\partial\epsilon_k}{\partial t} I_1\left(\frac{\lambda_k}{\Delta}\right) + \frac{2t}{J_{\text{H}}}\right] \stackrel{!}{=} 0, \tag{B9c}$$

$$\frac{1}{N}\frac{\partial F}{\partial \Phi} = \sum_k \frac{\partial\epsilon_k}{\partial\Phi} I_1\left(\frac{\lambda_k}{\Delta}\right) \stackrel{!}{=} 0. \tag{B9d}$$

We readily see that ground state solutions are given by $\Phi \in 2\pi\mathbb{Z}$. Then the first three equations yield cf. Eqs. (8):

$$3\pi q = \sum_k \delta_k = \delta_0 + 2\delta_{2\pi/3}, \tag{B10a}$$

$$T_{\text{K}}^3 = \prod_k \sqrt{\lambda_k^2 + \Delta^2} = \frac{\Delta^3}{\sin(\delta_3)\sin(\delta_{2\pi/3})^2}, \tag{B10b}$$

$$2(\delta_0-\delta_{2\pi/3}) = 3\frac{2\pi t}{J_{\rm H}} = \frac{2\pi}{J_{\rm H}}(\lambda_{2\pi/3}-\lambda_0)$$
$$= \frac{2\pi\Delta}{J_{\rm H}}[\cot(\delta_{2\pi/3})-\cot(\delta_0)]$$
$$= 2\sin(\delta_0-\delta_{2\pi/3})\frac{\pi T_{\rm K}}{J_{\rm H}}\sqrt[3]{\frac{1}{\sin(\delta_{2\pi/3})\sin^2(\delta_0)}}. \quad \text{(B10c)}$$

We readily recognize the Kondo solution $t=0$, $\delta_k=\pi q$, $\Delta = T_{\rm K}\sin(\pi q)$, which is present for any $T_{\rm K}/J_{\rm H}$. The last equation is the origin of Eq. (8c).

### 3. Finite temperatures

Of the presented finite temperature phases in Fig. 1(b) of the main text, the presence of the LFL and local moment phase is obvious. The existence of an LFL* and of the 3CK phase is discussed now by showing that there is a mean-field transition $T_{\rm SL} = J_{\rm H}q(1-q)$ below which $t$ develops a vacuum expectation value and a lower transition $T_{\rm K}^{\rm eff}$ at which $V$ spontaneously develops. For the perturbative solution in $\Delta$ at finite $T$, we use

$$n_f(\lambda) = I_1 = n_{\rm FD}(\lambda) = \frac{1-\tanh\left(\frac{\lambda}{2T}\right)}{2}, \quad \text{(B11)}$$

and perturbatively in $\Delta$,

$$I_2(\lambda) = T\sum_{\epsilon_n>0}\left(\frac{i}{i\epsilon_n-\lambda}+\frac{i}{i\epsilon_n+\lambda}\right)$$
$$\simeq \frac{\ln\left(\frac{D}{T}\right)}{\pi} - \frac{\psi^{(0)}\left(\frac{\frac{i\lambda}{T}+\pi}{2\pi}\right)+\psi^{(0)}\left(\frac{\pi-\frac{i\lambda}{T}}{2\pi}\right)}{2\pi}. \quad \text{(B12)}$$

The mean-field equations (perturbative in $\Delta$) are then

$$n_{\rm FD}(\lambda-2t) = q+\frac{2t}{J_{\rm H}} = q+\frac{\lambda}{J_{\rm H}}-\frac{\lambda-2t}{J_{\rm H}}, \quad \text{(B13)}$$
$$n_{\rm FD}(\lambda+t) = q-\frac{t}{J_{\rm H}}, \quad \text{(B14)}$$
$$3\ln\left(\frac{T_{\rm K}}{T}\right) = \sum_k\left[\frac{\psi^{(0)}\left(\frac{\frac{i\lambda_k}{T}+\pi}{2\pi}\right)+\psi^{(0)}\left(\frac{\pi-\frac{i\lambda_k}{T}}{2\pi}\right)}{2} - \frac{\psi^{(0)}\left(\frac{\frac{i\lambda_{t=0}}{T}+\pi}{2\pi}\right)+\psi^{(0)}\left(\frac{\pi-\frac{i\lambda_{t=0}}{T}}{2\pi.}\right)}{2}\right], \quad \text{(B15)}$$

with $\lambda_k = (\lambda+t,\lambda+t,\lambda-2t)$ and $\lambda_{t=0} = 2T\,\mathrm{artanh}(1-2q)$ the solution without $t$. The mean-field spin-liquid transition temperature is obtained by expanding the first two equations in $t$:

$$q = n_{\rm FD}(\lambda) \Leftrightarrow \lambda = 2T\,\mathrm{artanh}(1-2q), \quad \text{(B16)}$$
$$\frac{1}{J_{\rm H}} = -\frac{\partial n_{\rm FD}}{\partial\lambda} = \frac{1}{4T\cosh^2\left(\frac{\lambda}{2T}\right)}$$
$$= \frac{1}{4T\cosh^2[\mathrm{artanh}(1-2q)]}. \quad \text{(B17)}$$

Thus, for $0<q<\frac{1}{3}$:

$$\frac{T_{\rm SL}}{J_{\rm H}} = \frac{1}{4\pi\cosh^2[\mathrm{artanh}(1-2q)]} = q(1-q). \quad \text{(B18)}$$

For the solution of $T_{\rm K}^{\rm eff} < T_{\rm SL}$, it is more convenient to use

$$n_k = n_{\rm FD}(\lambda_k), \quad \text{(B19)}$$

and insert this into

$$3q = 2n_{2\pi/3}+n_0, \quad \text{(B20)}$$
$$\Delta n \equiv n_0 - n_{2\pi/3} = \frac{3t}{J_H} = \frac{T}{J_H}(\bar\lambda_{2\pi/3}-\bar\lambda_0). \quad \text{(B21)}$$

We use

$$\bar\lambda_{t=0} = \frac{\lambda_{t=0}}{T} = 2\mathrm{artanh}(1-2q), \quad \text{(B22)}$$
$$\bar\lambda_{2\pi/3} = \frac{\lambda_{2\pi/3}}{T} = 2\mathrm{artanh}(1-2n_{2\pi/3})$$
$$= 2\mathrm{artanh}\left(1-2q+\frac{2\Delta n}{3}\right), \quad \text{(B23)}$$
$$\bar\lambda_0 = \frac{\lambda_0}{T} = 2\mathrm{artanh}(1-2n_0)$$
$$= 2\mathrm{artanh}\left(1-2q-\frac{4\Delta n}{3}\right), \quad \text{(B24)}$$

to replace temperature in Eq. (B15):

$$T = T_{\rm K}\prod_k\left\{\exp\left[\frac{\psi^{(0)}\left(\frac{\frac{i\lambda_k}{T}+\pi}{2\pi}\right)+\psi^{(0)}\left(\frac{\pi-\frac{i\lambda_k}{T}}{2\pi}\right)}{2} - \frac{\psi^{(0)}\left(\frac{\frac{i\lambda_{t=0}}{T}+\pi}{2\pi}\right)+\psi^{(0)}\left(\frac{\pi-\frac{i\lambda_{t=0}}{T}}{2\pi}\right)}{2}\right]\right\}^{-1/3}$$
$$\equiv T_{\rm K}\underbrace{g[\lambda_{t=0},\lambda_{2\pi/3}(\Delta n),\lambda_0(\Delta n)]}_{:=f(\Delta n)}. \quad \text{(B25)}$$

We thus reduced the finite temperature Kondo transition in the presence of finite $t$, i.e., finite $\Delta n$ to a single equation for $\Delta n$:

$$\Delta n = \frac{T_K}{J_H} f(\Delta n)(\bar{\lambda}_{2\pi/3} - \bar{\lambda}_0). \tag{B26}$$

Numerical solution of this equation demonstrates the existence of $0 < T_K^{\rm eff} < T_{SL}$ for sufficiently small $T_K/J_H$.

#### 4. Landau free energy (perturbative in $t$)

We consider the case of small $t$ and employ $\xi = \lambda + i\Delta = T_K e^{i\pi q}$ [86]:

$$\begin{aligned} V(\Phi) &= \frac{N}{\pi}\sum_k \mathrm{Im}\left\{(\lambda_k + i\Delta)\ln\left[\frac{(\lambda_k+i\Delta)}{eT_K e^{i\pi q}}\right]\right\} \qquad \text{(B27)}\\ &= \frac{N}{\pi}\sum_k \mathrm{Im}\left(\sum_k \frac{\epsilon_k^2}{2\xi} - \frac{\epsilon_k^3}{6\xi^2} + \frac{\epsilon_k^4}{12\xi^3}\right)\\ &= \frac{T_K N}{\pi}\left[-3\bar{t}^2\sin(\pi q) - \cos(\Phi)\bar{t}^3\sin(2\pi q)\right.\\ &\quad \left. - \frac{3\bar{t}^4\sin(3\pi q)}{2}\right]. \qquad \text{(B28)}\end{aligned}$$

Up to the effect of biquadratic and ring exchange terms (see the following section), as well as the Hubbard-Stratonovich term $3t^2/J_H$, this expression yields Eq. (9) of the main text.

#### 5. Ring exchange and biquadratic terms

In the large $N$ limit, the transition between LFL and 3CK appears to be first order. Here, we consider additional terms which ultimately overcome the first-order behavior. We need

$$\begin{aligned}\langle f_m f_{m+1}^\dagger\rangle &\simeq -\int (d\epsilon)\frac{t_m}{[i\epsilon + \lambda + i\Delta\,\mathrm{sign}(\epsilon)]^2}\\ &= \frac{t_m}{\pi T_K}\sin(\pi q). \qquad \text{(B29)}\end{aligned}$$

We first study ring exchange terms of the form

$$H_3 = -\pi^2\frac{J_s}{N}d_{abc}\hat{S}_1^a\hat{S}_2^b\hat{S}_3^c - \pi^2\frac{J_\chi}{N}f_{abc}\hat{S}_1^a\hat{S}_2^b\hat{S}_3^c. \tag{B30}$$

These terms can be evaluated on mean-field level as ($T_{abc} = J_s d_{abc} + J_\chi f_{abc}$, and we use $t_m = te^{i\Phi/3}$)

$$\begin{aligned} H_3 &\simeq -\pi^2\frac{T_{abc}}{N}\langle f_1^\dagger\sigma^a f_1 f_2^\dagger\sigma^b f_2 f_3^\dagger\sigma^c f_3\rangle\\ &= \frac{T_{abc}(\sin\pi q)^3}{\pi T_K^3 N}[t_1t_2t_3\mathrm{tr}(\sigma^a\sigma^b\sigma^c) + \bar{t}_3\bar{t}_2\bar{t}_1\mathrm{tr}(\sigma^a\sigma^c\sigma^b)]\\ &= J_s(\sin\pi q)^3\frac{d_{abc}}{\pi T_K^3 N}\underbrace{\mathrm{tr}[\sigma^a(\sigma^b,\sigma^c)]}_{d_{abc}}t^3\cos(\Phi)\\ &\quad + J_\chi(\sin\pi q)^3\frac{if_{abc}}{\pi T_K^3 N}\underbrace{\mathrm{tr}[\sigma^a(\sigma^b,\sigma^c)]}_{if_{abc}}t^3\sin(\Phi)\\ &= N\frac{J_s(\sin\pi q)^3}{\pi T_K^3}t^3\cos(\Phi) + N\frac{J_\chi(\sin\pi q)^3}{\pi T_K^3}t^3\sin(\Phi). \end{aligned} \tag{B31}$$

We used

$$d_{abc}d_{abc} = N^2 - 4, \quad f_{abc}f_{abc} = N^2. \tag{B32}$$

This term enters $\beta$ in Eq. (9) of the main text.

We furthermore introduce biquadratic interactions:

$$H_4 = -\frac{\pi^3 J_4}{2N^3}\sum_m(\hat{S}_m^a\hat{S}_{m+1}^a)^2. \tag{B33}$$

Their mean-field decoupling leads to

$$\begin{aligned} H_4 &= -\frac{\pi^3 J_4}{2N^3}\left\langle\sum_m f_m^\dagger\sigma^a f_m f_{m+1}^\dagger\sigma^a f_{m+1} f_m^\dagger\sigma^b f_m f_{m+1}^\dagger\sigma^b f_{m+1}\right\rangle\\ &= 3t^4\frac{J_4\sin(\pi q)^4}{2N^3\pi T_K^4}\left\{\underbrace{\mathrm{tr}[\sigma^a(\sigma^a,\sigma^b)\sigma^b]}_{d_{abc}d_{abc}/2} + \underbrace{\mathrm{tr}(\sigma^a\sigma^a)^2}_{=(N^2-1)^2}\right\}\\ &\simeq N\frac{3J_4\sin(\pi q)^4}{2\pi T_K^4}t^4. \end{aligned} \tag{B34}$$

This term enters $\gamma$ in Eq. (9) of the main text.

For the plot of Fig. 2(c), we used $J_{\rm Ring}^{\rm eff} = 0.3$ and $J_4^{\rm eff} = 0.1$ in the effective replacement $J_H \to J_H(1 + dJ_{\rm ring}^{\rm eff} - d^2 J_4^{\rm eff})$ in the numerator of Eq. (8c), left.

The replacement is related to the microscopic Hamiltonian as follows. From the mean-field evaluation

$$\langle f_m f_{m+1}^\dagger\rangle = \sum_k \frac{\frac{G_k(0)}{3}}{3} = -\frac{d}{3\pi}. \tag{B35}$$

Therefore, on Hartree-Fock level,

$$H_3 \to -\frac{NJ_s\left(\frac{d}{3}\right)^3}{\pi} = N\pi^2 J_s\left(\frac{t}{J_H}\right)^3, \tag{B36}$$

$$H_4 \to \frac{NJ_4 3\left(\frac{d}{3}\right)^4}{2\pi} = \frac{NJ_4 3\pi^3\left(\frac{t}{J_H}\right)^4}{2}. \tag{B37}$$

For small $t/J_H$, this can be reinterpreted as a renormalization:

$$\frac{t^2}{J_H} \to \frac{t^2}{J_H\left[1 - \frac{\pi^2 J_s t}{J_H^2} - \frac{3\pi^2\left(\frac{t^2}{J_H^2}\right)J_4}{2}\right]} = \frac{t^2}{J_H\left[1 + \frac{\pi J_s}{J_H}\frac{d}{3} - \frac{J_4}{J_H}\frac{d^2}{3}\right]}. \tag{B38}$$

Hence, we identify

$$J_{\rm Ring}^{\rm eff} = \frac{\pi J_s}{3J_H}, \quad J_4^{\rm eff} = \frac{J_4}{3J_H}. \tag{B39}$$

## APPENDIX C: DYNAMICS OF GOLDSTONE MODES AND TOTAL FLUX

In this section, we derive the kinetic terms for Goldstone bosons and $\Phi(\tau)$, Eq. (12) of the main text.

#### 1. Goldstone bosons

Before turning to the effective action of Goldstone bosons, we comment on the structure

$$\frac{G}{H} = \frac{U(1)\times U(1)\times U(1)}{U(1)\times\mathbb{Z}_3}, \tag{C1}$$

of the Goldstone manifold. Smooth transformations of the large group $G$ are represented by three phases $\chi_m$:

$$f_m \to U_{mm'} f_{m'}; \quad c_m \to U_{mm'} c_{m'} \quad (U_{mm'} = \delta_{mm'} e^{i\chi_m}), \tag{C2}$$

and per definition $\chi_m(\tau = 1/T) = \chi_m(\tau = 0) + 2\pi j$. Following Appendix B, a convenient form of $U = \mathrm{diag}(e^{iA_1 - \Phi/3}, 1, e^{-iA_2+\Phi/3})$, as it cancels the fluctuating gauge fields on the links. To make the quotient group $G/H$ apparent, we factorize

$$U = e^{i\phi} V, \quad \text{with } \det V = 1. \tag{C3}$$

The naïve derivation of the Goldstone action implies the absorption the $V$ [i.e., the $SU(3)$ part of $G$] into $f, c$ at the expense of a Berry curvature term $\mathcal{A} = -iV^\dagger \partial_\tau V$. The integration of fermions then leads to an effective action in terms of $\mathcal{A}$, and thus implicitly in terms of $A_{1,2,3}$.

However, certain care is needed for this procedure. The quotient group introduces an emergent $\mathbb{Z}_3$ redundancy which is manifested in noncontractable loops ($j = 0, 1, 2$):

$$\exp\left[i\phi\left(\frac{1}{T}\right)\right] = \omega^j e^{i\phi(0)}, \tag{C4}$$

$$V\left(\frac{1}{T}\right) = \bar{\omega}^j V(0). \tag{C5}$$

The absorption of $f(\tau) = V(\tau)\tilde{f}(\tau)$ changes the boundary conditions [$\tilde{f}(1/T) = -\omega^j f(0)$], i.e., $\tilde{f}(\tau)$ is generically not a fermionic field. We conjecture that the topological nature of $\pi_1(G/H) = \mathbb{Z}_3$ is at the root of the ground state degeneracy of the 3CK phase.

To remedy this problem, we choose a parametrization of $U(\tau)$ such that the topological winding is manifest, i.e.,

$$\begin{aligned} U(\tau) = &\exp\left[i\bar{\phi}(\tau) + \frac{2\pi i \tau T}{3}\right] \\ &\times \begin{bmatrix} \exp\left(-\frac{2\pi i\tau T}{3}\right) & 0 & 0 \\ 0 & \exp\left(-\frac{2\pi i\tau T}{3}\right) & 0 \\ 0 & 0 & \exp\left(-\frac{4\pi i\tau T}{3}\right) \end{bmatrix} \\ &\times \bar{V}(\tau), \end{aligned} \tag{C6}$$

where both $e^{i\bar{\phi}(\tau)}$ and $\bar{V}(\tau)$ are periodic in imaginary time. In this parametrization, it is apparent that the three different $\mathbb{Z}_3$ sectors correspond to the $2\pi$ winding of one of the $\chi_m$. To derive the effective action of $V(\tau)$ fluctuations even for nonzero $j$, we thus absorb $e^{-i\bar{\phi}(\tau)}U(\tau)$ into fermionic fields (without changing their statistics) and integrate fermions subsequently (with $G_{cf}, G_{cf,k}$ the full Green's function of $c$ and $f$ space, $G_c, G_{c,k}$ the Green's function of conduction electrons, and $G, G_k$ the Green's function of $f$ electrons):

$$\frac{S(A_{2,3})}{N} = -\mathrm{Tr}\ln\left(-G_{cf}^{-1} + i\mathcal{A}\right) + \mathrm{tr}\ln\left(-G_c^{-1} + i\mathcal{A}\right) \tag{C7}$$

$$\simeq i\mathrm{Tr}(G_{cf}\mathcal{A}) - i\mathrm{tr}(G_c\mathcal{A}) - \frac{1}{2}\mathrm{Tr}[(G_{cf}\mathcal{A})^2] + \frac{1}{2}\mathrm{tr}[(G_c\mathcal{A})^2]. \tag{C8}$$

The symbol "tr" denotes a trace in the space of the three sites and in time, "Tr" additionally includes the $2 \times 2$ space of $c$ and $f$ electrons. Specifically, we employ a gauge in which

$$\mathcal{A}_{k'k} = \frac{2\pi jT}{3} + \underbrace{\frac{(\dot{A}_2 - \dot{A}_1)\delta_{kk'} + \left[\dot{A}_1 e^{i(k'-k)} - \dot{A}_2 e^{-i(k'-k)}\right]}{3}}_{=:\bar{\mathcal{A}}_{k'k}}. \tag{C9}$$

The leading term is fixed by the constraint $\sum_k \delta_k = 3\pi q$ (this result is true beyond mean field):

$$\begin{aligned} S^{(1)} &= i\int d\tau \sum_k G_k(\tau, \tau^+)\mathcal{A}_{kk}(\tau) \\ &= iQ\int d\tau \sum_k \mathcal{A}_{kk}(\tau) \\ &= iQ2\pi m. \end{aligned} \tag{C10}$$

Note that, since $Q \in \mathbb{Z}$, this expression is invariant, yields a trivial phase $2\pi$, and can be omitted.

Next, we switch to the term of second order in gradients, which can be expressed as

$$S^{(2)} = -\frac{N}{2}\int d\tau \sum_{kk'} I_{kk'}|\mathcal{A}_{kk'}|^2. \tag{C11}$$

The polarization operator under consideration is

$$\begin{aligned} I_{kk'} &= \int \frac{d\epsilon}{2\pi} \mathrm{tr}^{cf}[G_{cf,k}(\epsilon)G_{cf,k'}(\epsilon)] - G_{c,k}(\epsilon)G_{c,k'}(\epsilon) \\ &= [1 + 2(\pi\rho V)^2]\int \frac{d\epsilon}{2\pi} G_k(\epsilon)G_{k'}(\epsilon) \\ &= -\frac{1 + 2\rho\Delta}{J_\mathrm{H}} \begin{bmatrix} \frac{J_\mathrm{H}\sin(\delta_+)^2}{\Delta\pi} & \frac{J_\mathrm{H}\sin(\delta_+)^2}{\Delta\pi} & 1 \\ \frac{J_\mathrm{H}\sin(\delta_+)^2}{\Delta\pi} & \frac{J_\mathrm{H}\sin(\delta_+)^2}{\Delta\pi} & 1 \\ 1 & 1 & \frac{J_\mathrm{H}\sin(\delta_0)^2}{\Delta\pi} \end{bmatrix}_{kk'}. \end{aligned} \tag{C12}$$

We here used the short-hand notation $\delta_+ = \delta_{2\pi/3}$ and that

$$\begin{aligned} &\int \frac{d\epsilon}{2\pi} G_k(\epsilon)G_{k'}(\epsilon) \\ &= -\frac{1}{\pi} \begin{cases} \frac{\Delta}{\Delta^2 + \lambda_k^2}, & \lambda_k = \lambda_{k'} \\ \frac{\pi + \arctan\left(\frac{\Delta}{\lambda_k}\right) - \arctan\left(\frac{\Delta}{\lambda_{k'}}\right)}{\lambda_{k'} - \lambda_k}, & \lambda_k < 0, \lambda_{k'} > 0, \end{cases} \end{aligned} \tag{C13}$$

as well as the mean-field equations, Eq. (B10). It is important to realize that remnant $U(1)$ terms and $SU(3)$ terms in Eq. (C11) decouple

$$S^{(2)} = -\frac{N}{2}\int d\tau \sum_{kk'}\left[I_{kk'}|\bar{\mathcal{A}}_{kk'}|^2 + I_{kk}\left(\frac{2\pi mT}{3}\right)^2 \delta_{kk'}\right]. \tag{C14}$$

The second term yields a vanishing contribution to the weight in the limit $T \to 0$ and is disregarded. We further use that

$$|\bar{\mathcal{A}}_{kk'}|^2 = \frac{\sum_m \dot{A}_m^2}{18}. \tag{C15}$$

Here, we have used a gauge transformation to return to the generic gauge. The combination of Eqs. (C12), (C14), and (C15) results in the final result, Eq. (12b) in the main text. To obtain Eq. (15), we employ the parametrization in terms of unit vectors $\hat{e}_m$ and $\sum_m \hat{e}_m \hat{e}_m^T = 31$.

### 2. Total flux

To obtain the dynamics of the total flux $\Phi(\tau)$, we use the notation $\delta\lambda_k = -2t[\cos(k+\Phi/3) - \cos(k)]$ and expand the fermionic determinant to second order in $\delta\lambda_k$.

$$\begin{aligned} S_{\text{eff}}^{(2)} &\simeq \frac{N}{2}\sum_{\omega_m,k}\delta\lambda_k(\omega_m)\delta\lambda_k(-\omega_m)\sum_{\epsilon_n}G_k(\epsilon_n)G_k(\epsilon_n+\omega_m) \\ &\overset{T\to 0}{\simeq} \frac{N\Delta}{2\pi T}\sum_{\omega_m,k}\delta\lambda_k(\omega_m)\delta\lambda_k(-\omega_m)\frac{\ln\left[\frac{\lambda_k^2+\Delta^2}{\lambda_k^2+(\Delta+|\omega|)^2}\right]}{|\omega|(2\Delta+|\omega|)} \\ &= \frac{N\Delta}{2\pi T}\sum_{\omega_m,k}\delta\lambda_k(\omega_m)\delta\lambda_k(-\omega_m) \\ &\quad\times\begin{cases}\left[-\frac{1}{\Delta^2+\lambda_k^2}+|\omega|\frac{\Delta}{(\Delta^2+\lambda_k^2)^2}\right], & |\omega|\ll\lambda_k^2+\Delta^2, \\ -\frac{\ln\left(\frac{\omega^2}{\lambda_k^2+\Delta^2}\right)}{\omega^2}, & |\omega|\gg\lambda_k^2+\Delta^2.\end{cases} \end{aligned} \tag{C16}$$

The equation substantially simplifies for small $t \ll \lambda$ and leads to the kinetic energy of $\Phi$ fluctuations:

$$\begin{aligned} S_{\text{kin}}(\Phi) &= N\frac{3t^2T_{\text{K}}\sin(\pi q)}{4\pi T}\sum_{\omega_m}\Phi(\omega_m)\Phi(-\omega_m) \\ &\quad\times\begin{cases}|\omega|\frac{\sin(\pi q)}{T_{\text{K}}^3}, & |\omega|\ll T_{\text{K}}^2, \\ \left[\frac{1}{T_{\text{K}}^2}-\frac{\ln\left(\frac{\omega^2}{T_{\text{K}}^2}\right)}{\omega^2}\right], & |\omega|\gg T_{\text{K}}^2.\end{cases} \end{aligned} \tag{C17}$$

The $|\omega|$ term in the first line is the origin of the damped kinetic term presented in the main text and leads to logarithmic correlators.

### 3. Estimate of tunneling time and tunneling action

As demonstrated in the main text, details of the tunneling rate $\Gamma$ are irrelevant for the transition. We therefore constrain ourselves to merely estimate $\Gamma$, based on a tunneling event

$$\begin{aligned} \Phi(\tau) &= \frac{\pi}{2}+\frac{2\pi\tau}{\tau_0\theta\left(\tau_0^2-4\tau^2\right)} \\ &\Rightarrow |\Phi(\omega)|^2 = \frac{\left[\omega\tau_0\cos\left(\frac{\omega\tau_0}{2}\right)-2\sin\left(\frac{\omega\tau_0}{2}\right)\right]^2}{(\omega\tau_0)^4}. \end{aligned} \tag{C18}$$

In terms of dimensionless parameters $\bar{t} = t/T_{\text{K}}$ and $\bar{\tau}_0 = \tau_0/T_{\text{K}}$, $\bar{\omega} = \omega\tau_0$, $\Phi(\omega) = \bar{\Phi}(\omega\tau_0)$, we obtain

$$\begin{aligned} \frac{S_{\text{tun}}(\bar{\tau}_0)}{N} &\sim \beta\bar{\tau}_0+\bar{t}^2\sin(\pi q)\bar{\tau}_0\int_0^\infty|\bar{\Phi}(\bar{\omega})|^2\left(1-\frac{\ln\{[\sin(\pi q)+\bar{\omega}]^2\bar{\tau}_0^2\}}{\bar{\omega}^2\bar{\tau}_0^2}\right) \\ &\sim \beta\bar{\tau}_0\left[1+\frac{\bar{t}^2\sin(\pi q)}{\beta}\left(\frac{\pi}{6}-\frac{1}{\bar{\tau}_0^2}\left\{\frac{\pi\ln\left[\sin(\pi q)^2\bar{\tau}_0^2\right]}{60}+0.7\right\}\right)\right]. \end{aligned} \tag{C19}$$

To obtain the optimal tunneling time, we use that $\bar{t} \sim \beta/\gamma$ at the mean-field first-order transition. We thus obtain, for any $q$ such that $\sin(\pi q) \sim 1$:

$$\tau_0^{\text{optimal}} \sim \frac{1}{T_{\text{K}}}\begin{cases}1, & \gamma\ll 1, \\ \sqrt{\frac{\ln(\gamma)}{\gamma}}, & \gamma\gg 1,\end{cases} \tag{C20}$$

$$\frac{S_{\text{tun}}}{N} \sim \beta\begin{cases}\frac{1}{\gamma}+1.4, & \gamma\ll 1, \\ \sqrt{\frac{\ln(\gamma)}{\gamma}}, & \gamma\gg 1,\end{cases} \tag{C21}$$

as quoted in the main text.

### 4. Implications for interwire correlations

Using $\psi = (c, f)^T$, the generating functional at mean-field level, but including fluctuations of the Goldstone modes, is $Z = \prod_k Z_k$:

$$\begin{aligned} Z_k(\eta) &= \int\mathcal{D}\psi_k\exp\Big[-\int d\tau\,\bar{\psi}_k(-\hat{G}^{-1}+i\mathcal{A})\psi_k \\ &\quad+\bar{\psi}_k U\eta_k+\bar{\eta}_k U^\dagger\psi_k\Big] \\ &= \exp\Big[\int d\tau\,\bar{\eta}_k\hat{G}\eta_k+S(A_{2,3})\Big]. \end{aligned} \tag{C22}$$

Here, $U$ is the diagonal matrix introduced after Eq. (B2). Intersite correlators (obtained by differentiation with respect to $\eta$) thus contain averages like the following:

$$\begin{aligned} \langle e^{iA_m(\tau)}e^{-iA_{m'}(0)}\rangle &= \text{tr}[e^{-(\beta-\tau)H}e^{-iA_m}e^{-\tau H}e^{iA_{m'}}] \\ &\overset{T\to 0}{=} \sum_{\mathbf{p}}\int d^2x\int d^2x'\psi_0^*(\vec{x})e^{-iA_m(\vec{x})} \\ &\quad\times\psi_{\vec{p}}(\vec{x})e^{-i\tau\epsilon_{\vec{p}}}\psi_{\vec{p}}^*(\vec{x}')e^{iA_{m'}(\vec{x}')}\psi_0(\vec{x}') \\ &= \delta_{mm'}\exp(-i\epsilon_{-2\hat{e}_m/3}). \end{aligned} \tag{C23}$$

We used the notation $\psi_{\vec{p}}(\vec{x})$ for eigenstates of $(-i\nabla_{\vec{x}})^2/(2m_x)$ with eigenenergy $\vec{p}^2/(2m_x)$. Thus, only intrasite terms survive.

### 5. Ordering of $\mathcal{O}_s = d_{abc}\hat{S}_1^a\hat{S}_2^b\hat{S}_3^c$.

For $t > t_c$ (i.e., in the 3CK phase), the effective action of $\Phi$ fluctuations can be obtained by expansion about the minimum of $\cos(\Phi)$ leading to

$$S(\Phi) = \int\frac{d\omega}{2\pi}\Phi(\omega)\Phi(-\omega)\left(\frac{\eta}{4\pi}|\omega|+\frac{M_\Phi}{2}\right), \tag{C24}$$

where $M_\Phi = N\beta T_K$. The correlator of phase fluctuations thus decays as

$$\langle \Phi(\tau)\Phi(0)\rangle \sim \int_0^\infty d\omega \frac{\cos(\omega\tau)}{\eta|\omega| + 2\pi M_\Phi} \sim -\frac{\eta \sin(2\pi M_\Phi \tau)}{(M_\Phi \tau)^2}, \tag{C25}$$

and therefore leads to long-range correlations:

$$\langle \mathcal{O}_s(\tau)\mathcal{O}_s(0)\rangle \sim \frac{t^6}{T_K^6}\exp\left[-\frac{\eta \sin(2\pi M_\Phi \tau)}{(M_\Phi \tau)^2}\right] \to \frac{t^6}{T_K^6}. \tag{C26}$$

## APPENDIX D: PHASE SLIPS

Here, we include phase slips of weight $\Gamma$ and time $\tau_0$, which is assumed to be smaller than all other time scales of the effective theory. We now consider a single kink in $\Phi$ with shift $2\pi$, which is associated with an amplitude [87]

$$\mathcal{A}^{(0)}_{(-\tau/2,\Phi)\to(\tau/2,\Phi\pm 2\pi)} = \Gamma \int_{-\tau/2}^{\tau/2} d\tau_c. \tag{D1}$$

### 1. Instanton interactions

We consider the full partition function (generating functional) to second order in $\Gamma$:

$$Z(\eta) = Z_0(\eta) + \Gamma^2 \sum_{\pm} \int_0^\beta d\tau_f \int_0^{\tau_i} d\tau_i Z_{2,\pm}(\eta;\tau_f,\tau_i), \tag{D2}$$

where a phase slip (antiphase slip) is introduce at $\tau_i$ ($\tau_f$), and the sum over $\pm$ indicates the direction of the slip. The partition function is

$$\begin{aligned} F &= -T\ln Z(0) \\ &\simeq \underbrace{-T\ln Z_0(0)}_{=F_0} - T\Gamma^2 \sum_{\pm}\int_0^\beta d\tau_f \int_0^{\tau_i} d\tau_i \frac{Z_{2,\pm}(0;\tau_f,\tau_i)}{Z_0(0)}. \end{aligned} \tag{D3}$$

We use that, before and after a phase slip, $h$ labels the same quantum states; however, their energy has been shuffled around cyclically $\epsilon_h \to \epsilon_{h+1}$. We can thus express the partition function in the helicity basis, $Z_0(\eta) = \prod_h Z_{0,h}(\eta_k)$, $Z_{2,\pm}(\eta;\tau_f,\tau_i) = \prod_h Z_{2,\pm,h}(\eta_h;\tau_f,\tau_i)$, where ($h$ index from now on suppressed unless explicitly restored)

$$Z_0(\eta) = \int \mathcal{D}(c,f)\exp\left[-\int d\tau(\bar{c},\bar{f})(\partial_\tau + H_{\rm MF})(c,f)^T + \bar{\eta}f + \bar{f}\eta\right], \tag{D4a}$$

$$Z_2(\eta) = \int \mathcal{D}(c,f)\exp\left\{-\int d\tau(\bar{c},\bar{f})[\partial_\tau + H_{\rm slips}(\tau)](c,f)^T + \bar{\eta}f + \bar{f}\eta\right\}, \tag{D4b}$$

and

$$H_{\rm slips}(\tau) = \begin{bmatrix} \epsilon(\mathbf{p}) & V \\ V & \lambda(\tau) \end{bmatrix}, \tag{D4c}$$

where $\lambda(\tau) = \lambda + \delta\lambda\chi_{\tau_i,\tau_f}(\tau)$ and $\chi_{\tau_i,\tau_f}(\tau) = 1$ for $\tau_i < \tau < \tau_f$, and $\chi_{\tau_i,\tau_f}(\tau) = 0$ otherwise. Note that $\lambda = \lambda_h = \lambda - \epsilon_h$; for the ground state, $\delta\lambda = 3t$; for one of the excited states, $\delta\lambda = -3t$; and for the third state, $\delta\lambda = 0$ ($k = \pm 2\pi/3$ are degenerate).

Thus, the instantons generate an x-ray edge problem in each helicity channel. We follow Ref. [88] and employ the long-time $f$-electron Green's function:

$$G_f(\tau) \sim -\frac{g}{\tau}, \tag{D5}$$

with $g = \Delta/\pi(\Delta^2 + \lambda^2)$ for the Kondo/resonant level problem. This leads to

$$S_{\rm slips}(\tau_f - \tau_i) = (\tau_f - \tau_i)\delta\lambda G_f(0,0^+) + \left(\frac{\delta_x}{\pi}\right)^2 \ln\left(\frac{\tau_f - \tau_i}{\lambda}\right), \tag{D6}$$

where $\delta_x = -\arctan(\pi g \delta\lambda)$. The first (classical) term cancels upon taking the product of $h$, leaving only the logarithmic repulsion. This concludes the derivation of $\kappa = 2N(\delta_x/\pi)^2$, Eq. (19), as presented in the main text.

### 2. Infinite order resummation of phase slips

We now switch to the full resummation of phase slips. We consider an amplitude for $\Phi \to \Phi + N_\Phi 2\pi$ and denote $n$ and $\bar{n}$ the number of kinks/antikinks (i.e., $n - \bar{n} = N_\Phi$) and their center of mass time $\tau_1, \ldots \tau_{n+\bar{n}}$. Different instanton sequences correspond to the integral over these variables. Then the amplitude is

$$\begin{aligned} \mathcal{A}_{(0,\Phi)\to(\beta,\Phi+N_\Phi 2\pi)} = \sum_{n=0}^\infty \sum_{\bar{n}=0}^\infty \delta_{n-\bar{n},N_\Phi}\, \Gamma^{n+\bar{n}} \sum_{\substack{\text{perm. of} \\ \bar{n},\, n \text{ kinks}}} \Bigg( \int_0^\beta d\tau_{n+\bar{n}} \cdots \int_0^{\tau_3} d\tau_2 \int_0^{\tau_2} d\tau_1 \\ \times \mathrm{tr}\left\{ \exp\left[-\int_{\tau_{n+\bar{n}}}^\beta d\tau' \hat{H}_{\rm MF}(\Phi + N_\Phi 2\pi)\right] \ldots \exp\left[-\int_{\tau_1}^{\tau_2} d\tau' \hat{H}_{\rm MF}(\Phi \pm 2\pi)\right] e^{-\int_{\tau_0}^{\tau_1} d\tau' \hat{H}_{\rm MF}(\Phi)} \right\} \Bigg). \end{aligned} \tag{D7}$$

In the second line, the $\pm$ refers to the sign of the first kink. We can now use that the Hamiltonian between two kinks is time independent, and the evolution operator between two kinks is

$$\begin{aligned}\mathcal{T}\exp\left[-\int_{\tau_l}^{\tau_{l+1}} d\tau' \hat{H}_{\mathrm{MF}}(\Phi + k2\pi)\right] &= \prod_{\Delta\tau}[1 + \Delta\tau \hat{H}(\Phi + k2\pi)] \\ &= \prod_{\Delta\tau}\left\{\tau_\Phi^k[1 + \Delta\tau H(\Phi)]\tau_\Phi^{-k}\right\} \\ &= \tau_\Phi^k \prod_{\Delta\tau}\{[1 + \Delta\tau H(\Phi)]\}\tau_\Phi^{-k} \\ &= \tau_\Phi^k \mathcal{T}\left\{\exp\left[-\int_{\tau_l}^{\tau_{l+1}} d\tau' H_{\mathrm{MF}}(\Phi)\right]\right\}\tau_\Phi^{-k}. \end{aligned} \tag{D8}$$

Thus, a kink at time $\tau$ is represented by the operator insertion $\tau_\Phi$ at time $\tau$ into the partition sum

$$\begin{aligned}\mathcal{A}_{(0,\Phi)\to(\beta,\Phi+N_\Phi 2\pi)} &= \sum_{n=0}^{\infty}\sum_{\bar{n}=0}^{\infty} \delta_{n-\bar{n},N_\Phi}\, \Gamma^{n+\bar{n}} \frac{(n+\bar{n})!}{n!\bar{n}!}\frac{1}{(n+\bar{n})!} \\ &\quad \times \mathcal{T}\left\{\int_0^\beta d\tau_n \cdots \int_0^\beta d\tau_1 \int_0^\beta d\bar{\tau}_{\bar{n}} \cdots \int_0^\beta d\bar{\tau}_1 \mathrm{tr}\left[\prod_{j=1}^{n}\prod_{\bar{j}=1}^{\bar{n}} \tau_\Phi(\tau_k)\tau_\Phi^{-1}(\bar{\tau}_{\bar{j}}) \exp\left(-\int_0^\beta d\tau \hat{H}_{\mathrm{MF}}\right)\right]\right\} \\ &= \frac{1}{3}\sum_\theta e^{-i\theta N_\Phi} \mathrm{tr}\left\{\exp\left[\int_0^\beta d\tau \Gamma e^{i\theta}\tau_\Phi(\tau)\right]\exp\left[\int_0^\beta d\tau \Gamma e^{-i\theta}\tau_\Phi^{-1}(\tau)\right]\exp\left[-\int_0^\beta d\tau \hat{H}_{\mathrm{MF}}\right]\right\}. \end{aligned} \tag{D9}$$

We used the Fourier transform on $\ell^3$ with periodic boundary conditions (i.e., with possible wave vectors $\theta = 0, \pm 2\pi/3$) such that $\sum_\theta e^{i\theta N} = 3\delta_{N,0}$ and $\sum_n e^{in\theta} = 3\delta_{\theta,0}$. Here, $\frac{(n+\bar{n})!}{n!\bar{n}!}$ is the number of possibilities to arrange the $n$ upsteps if there are $n+\bar{n}$ steps in total. The factor $\frac{1}{(n+\bar{n})!}$ accounts for the fact that the integration domain has been increased from an explicitly time-ordered $n+\bar{n}$-dimensional integral in Eq. (D7), to an $n+\bar{n}$-dimensional hypercube.

The total partition sum is given by (we use $\sum_{N_\Phi} e^{-iN_\Phi\theta} = 3\delta_{\theta,0}$ for $N_\Phi = 0, \pm 1$)

$$\begin{aligned} Z &= \sum_{N_\phi} \mathcal{A}_{(0,\Phi)\to(\beta,\Phi+N_\Phi 2\pi)} \\ &= \mathrm{tr}\big(\exp\{-\beta[\hat{H}_{\mathrm{MF}} - \Gamma(\tau_\Phi + \tau_\Phi^{-1})]\}\big). \end{aligned} \tag{D10}$$

We now restore the matrix space of different vacua. In total, we obtain

$$\begin{aligned} H_{\mathrm{eff}} &= \sum_x [-t_c c_{\alpha m}^\dagger(x) c_{\alpha m}(x+1) + \mathrm{H.c.} - \mu c_{\alpha m}^\dagger(x) c_{\alpha m}(x)]1_\Phi \\ &\quad + (t\sigma_\Phi f_{\alpha,m}^\dagger f_{\alpha,m+1} + \mathrm{H.c.}) + \lambda f_{\alpha m}^\dagger f_{\alpha m} 1_\Phi \\ &\quad + (V f_{\alpha,m}^\dagger c_{\alpha,m} + \mathrm{H.c.})1_\Phi - \Gamma(\tau_\Phi + \tau_\Phi^{-1}). \end{aligned} \tag{D11}$$

This concludes the derivation of Eq. (17) of the main text.

### 3. Orthogonality catastrophe using bosonization

We start from the effective Hamiltonian derived in the previous section

$$H = H_0 + H_\Gamma, \quad H_\Gamma = -\Gamma\hat{O}, \quad \hat{O} = \tau_\Phi + \tau_\Phi^{-1}. \tag{D12}$$

We are going to treat this problem perturbatively to the second order in $\Gamma$ and diagonalize $H_0$ in the helicity $h$ basis. Then considering that $\lambda_h(\Phi)$ is different for $\Phi = -2\pi, 0, 2\pi$, we have

$$\begin{aligned} H_0 &= \sum_{\Phi=0}\sum_h |\Phi\rangle H_{0h}(\Phi) \langle\Phi|, \\ H_{0h}(\Phi) &= \begin{pmatrix} c \\ f \end{pmatrix}_h^\dagger \begin{bmatrix} \epsilon_c & V \\ V & \lambda_h(\Phi) \end{bmatrix} \begin{pmatrix} c \\ f \end{pmatrix}_h. \end{aligned} \tag{D13}$$

Note that $c$ electrons have another momentum $k$ along the wires, which is implicit here. This problem as is, is difficult to treat. We are forced to (i) go to the scattering basis $\psi_{h\sigma}$ and (ii) assume that the phase shift is independent of the energy, i.e., the electrons in scattering basis experience a potential scattering $\tilde{V}_h(\Phi)$, which depends on the flux $\Phi$. In that case, we can unfold the conduction electrons to right movers only and write

$$\begin{aligned} H_{0h}(\Phi) &= H_{0h} + \sqrt{2\pi}\tilde{V}_h(\Phi)\psi_{h\sigma}^\dagger(0)\psi_{h\sigma}(0), \\ H_{0h} &= -iv_F \int dx \psi_{h\sigma}^\dagger \partial_x \psi_{h\sigma}, \end{aligned} \tag{D14}$$

where the relation between the potential scattering $\tilde{V}_h(\Phi)$ and the phase shift is shown below in Eq. (D18), and the factor of $\sqrt{2\pi}$ is introduced for future convenience. Next, we bosonize, i.e., express the fermions as

$$\psi_h(x) \sim e^{i\sqrt{2\pi}\varphi_h(x)}, \quad [\varphi_h(x), \varphi_{h'}(y)] = \frac{i}{2}\mathrm{sgn}(x-y)\delta_{hh'}. \tag{D15}$$

The Hamiltonian becomes

$$H_{0h}(\Phi) = H_{0h} + (\partial_x \varphi_h)\tilde{V}_h(\Phi), \quad H_{0h} = \frac{v_F}{2}\int_0^\infty dx(\partial_x\varphi_h)^2. \tag{D16}$$

It is easy to see that the potential scattering term can be eliminated

$$H_{0h}(\Phi) \equiv \frac{v_F}{2}\int dx\left[\partial_x\varphi_h + \frac{\delta(x)\tilde{V}_h(\Phi)}{v_F}\right]^2, \text{ i.e., } \quad \varphi_h(x) \to \varphi_h(x) + \frac{\theta(x)\tilde{V}_h(\Phi)}{v_F}. \tag{D17}$$

By plugging this into $\psi \sim e^{i\sqrt{2\pi}\varphi}$, we can see that this corresponds to the phase shift:

$$\psi_{\text{out},h} = \psi_{\text{in},h}e^{2i\delta_h}, \quad \delta_h = \sqrt{\frac{\pi}{2}}\frac{\tilde{V}_h}{v_F}. \tag{D18}$$

Each flux configuration corresponds to a different phase shift in a given helicity sector, and these configurations are related to each other via the so-called Schotte-Schotte transformation [89]:

$$U_h(\Phi, \Delta\Phi) = \exp\left\{-\frac{i\varphi(0)\left[\tilde{V}_h(\Phi+\Delta\Phi) - \tilde{V}_h(\Phi)\right]}{v_F}\right\}. \tag{D19}$$

Using the commutation relation of bosons and the fact that $e^{sX}Ye^{-sX} = Y + s(X, Y)$, for $(X, Y)$ $c$ number, we can check that

$$H_{0h}(\Phi+\Delta\Phi) = U_h^\dagger(\Phi, \Delta\Phi)H_{0h}(\Phi)U_h(\Phi, \Delta\Phi) \tag{D20}$$

$$= H_{0h} + (\partial_x\varphi)\tilde{V}_h(\Phi) - i[\tilde{V}(\Phi+\Delta\Phi) - \tilde{V}(\Phi)]\int_x \partial_x\varphi[\varphi(0), \partial_x\varphi]$$

$$= H_{0h} + \tilde{V}(\Phi+\Delta\Phi)(\partial_x\varphi)|_{x=0}. \tag{D21}$$

Going to the interaction picture with regard to $H_0$ and expanding the partition function in $\Gamma$, we have

$$\begin{aligned}
\frac{Z}{Z_0} &= \left\langle T_\tau \exp\left[-\int_{-1/2T}^{1/2T} d\tau H_\Gamma(\tau)\right]\right\rangle_0 \\
&= 1 + \frac{\Gamma^2}{2}\int d\tau_1 d\tau_2 \,\langle T_\tau \exp(\tau_1 H_0)\hat{O}\exp[(\tau_2-\tau_1)H_0]\hat{O}\exp(-\tau_2 H_0)\rangle_0 \\
&= 1 + \frac{\Gamma^2}{2}\int d\tau_1 d\tau_2 \,\langle T_\tau \exp[(\tau_1-\tau_2)H_0]\exp[(\tau_2-\tau_1)\hat{O}H_0\hat{O}]\rangle_0 \\
&= 1 + \frac{\Gamma^2}{2}\sum_\Phi\sum_{\alpha=\pm1}\int d\tau_1 d\tau_2 \prod_h \langle T_\tau \exp[(\tau_1-\tau_2)H_{0h}(\Phi)]\exp[(\tau_2-\tau_1)H_{0h}(\Phi+2\pi\alpha)]\rangle_0 ,
\end{aligned} \tag{D22}$$

where $\hat{O} = \tau^{+1} + \tau^{-1}$, we used that the linear-in-$\Gamma$ term vanishes due to trace and used the cyclic property of the trace with the Boltzmann factor $e^{-\beta H_0}/Z_0$ to shuffle the time-evolutions. Using Eq. (D20),

$$\exp[\tau H_{0h}(\Phi+\Delta\Phi)] = U_h^\dagger(\Phi, \Delta\Phi)\exp[\tau H_{0h}(\Phi)]U_h(\Phi, \Delta\Phi), \tag{D23}$$

we can write

$$\begin{aligned}
&\langle T_\tau \exp[-\Delta\tau H_{0h}(\Phi)]U_h^\dagger(\Phi, \Delta\Phi)\exp[\tau H_{0h}(\Phi)]U_h[\Phi, \Delta\Phi]\rangle_0 \\
&\quad = \langle T_\tau U_h^\dagger(\Phi, \Delta\Phi; \tau)U_h(\Phi, \Delta\Phi)\rangle_0 \\
&\quad = \left\langle T_\tau \exp\left[\frac{i\varphi(\tau)\Delta V_h(\Phi, \Delta\Phi)}{v_F}\right]\exp\left[\frac{-i\varphi(0)\Delta V_h[\Phi, \Delta\Phi]}{v_F}\right]\right\rangle \\
&\quad \sim |\tau|^{-[\Delta\tilde{V}_h(\Phi, \Delta\Phi)]^2/2\pi v_F^2},
\end{aligned} \tag{D24}$$

where we used that

$$\langle e^{i\gamma\varphi(\tau)}e^{-i\gamma\varphi(0)}\rangle = \frac{1}{|\tau|^{\gamma^2/2\pi}}. \tag{D25}$$

As a reminder, $\Delta\tilde{V}_h$ can be related to the phase shift

$$\begin{aligned}
\Delta\tilde{V}_h(\Phi, \Delta\Phi) &\equiv \tilde{V}_h(\Phi+\Delta\Phi) - \tilde{V}_h(\Phi) \\
&= v_F\sqrt{\frac{2}{\pi}}[\delta_h(\Phi+\Delta\Phi) - \delta_h(\Phi)],
\end{aligned} \tag{D26}$$

which leads to

$$\frac{Z}{Z_0} = 1 + \frac{1}{T}\Gamma^2 \sum_{\Phi} \sum_{\alpha=\pm 1} \int_{-1/2T}^{1/2T} d\Delta\tau |\Delta\tau|^{-\kappa},$$

$$\kappa = \sum_h \left[ \frac{\delta_h(\Phi + \Delta\Phi)}{\pi} - \frac{\delta_h(\Phi)}{\pi} \right]^2. \tag{D27}$$

Up to subleading terms in small $t$ (which are not important near the transition), this exactly reproduces Eq. (D6). The time integral leads to

$$\frac{Z}{Z_0} = 1 + \mathcal{C}'\Gamma^2 T^{\kappa-2}, \tag{D28}$$

where $\mathcal{C}'$ is a constant. The correction to free energy $F_0 = -T \log Z_0$ is

$$F - F_0 = -\mathcal{C}'\Gamma^2 T^{\kappa-1}. \tag{D29}$$

#### 4. $\langle \sigma_\Phi(\tau)\sigma_\Phi(0)\rangle$ correlation function

In this section, we compute the correlator $\langle \sigma_\Phi(\tau)\sigma_\Phi(0)\rangle$, which is related to the order parameter $\langle \mathcal{O}_s(\tau)\mathcal{O}_s(0)\rangle$ or $\langle \Phi(\tau)\Phi(\tau)\rangle$ in this paper, within the $t-\Gamma$ Hamiltonian $H = H_0 + H_\Gamma$. In the $\Gamma/t \gg 1$ regime (FL phase), this is exponentially decaying. This can be seen easily in a basis in which the $-\Gamma O$ term is diagonal. In the limit of large $\Gamma$, we can use a unitary transformation $U_O$ to diagonalize $O$:

$$O = \tau_\Phi + \tau_\Phi^{-1} = \begin{pmatrix} 0 & 1 & 1 \\ 1 & 0 & 1 \\ 1 & 1 & 0 \end{pmatrix} \to U_O^\dagger O U_O = \begin{pmatrix} -1 & & \\ & -1 & \\ & & 2 \end{pmatrix}, \tag{D30}$$

and go to the interaction picture with regard to $-\Gamma\tau^x$. In this picture, $\sigma(\tau)$ is time dependent and is given by

$$\rho_\Gamma = \frac{\exp\left(-\frac{\Gamma}{T}\right)}{2\exp\left(-\frac{\Gamma}{T}\right) + \exp\left(\frac{2\Gamma}{T}\right)} \begin{bmatrix} 1 & & \\ & 1 & \\ & & \exp\left(\frac{3\Gamma}{T}\right) \end{bmatrix} \to \begin{bmatrix} 0 & & \\ & 0 & \\ & & 1 \end{bmatrix},$$

$$\sigma_\Gamma(\tau) = \frac{\omega^2}{2} \begin{pmatrix} 1 & i & -x^{-1}\sqrt{2} \\ i & -1 & ix^{-1}\sqrt{2} \\ -x\sqrt{2} & ix\sqrt{2} & 0 \end{pmatrix}, \tag{D31}$$

in terms of $x = e^{3\tau\Gamma}$. With this density matrix $\mathrm{tr}(\rho_\Gamma O) = o_{33}$. Therefore, to the leading order in tunneling $t$,

$$\langle \sigma_\Gamma \rangle = \langle T_\tau \sigma_\Gamma(\tau)\sigma_\Gamma(0)\rangle = 0,$$
$$\langle T_\tau \sigma_\Gamma(\tau)\sigma_\Gamma^\dagger(0)\rangle = \langle T_\tau \sigma_\Gamma^\dagger(\tau)\sigma_\Gamma(0)\rangle = e^{-3|\tau|\Gamma}. \tag{D32}$$

This is the origin of the fact that $t$ is irrelevant in the $\Gamma/t \gg 1$ regime, within the $t-\Gamma$ Hamiltonian. In the opposite regime of $\Gamma/t \ll 1$, we can use the same technique as in the previous section to compute the correlators. Since $\sigma_\Phi$ commutes with $H_0$, to zero order in $\Gamma$, we have

$$\langle \sigma_\Phi(\tau)\sigma_\phi^\dagger(0)\rangle = \tfrac{1}{3}\mathrm{tr}(\sigma_\Phi\sigma_\phi^\dagger) = 1. \tag{D33}$$

To second order in $\Gamma$, we have (we have neglected the disconnected part since it does not depend on $\tau$)

$$\langle \sigma_\Phi(\tau)\sigma_\phi^\dagger(0)\rangle = 1 + \Gamma^2 \int_{-1/2T}^{1/2T} d\tau_1 d\tau_2 \langle T_\tau \sigma_\Phi(\tau)\sigma_\Phi^\dagger(0)\hat{O}(\tau_1)\hat{O}(\tau_2)\rangle. \tag{D34}$$

We can divide the integration range into six configurations (assuming $\tau_1 > \tau_2$):

$$\theta_1 \equiv \theta(\tau_1 > \tau_2 > \tau > 0): \quad \sum_{\alpha\alpha'} \langle e^{\tau_1 H_0}\tau_\Phi^\alpha e^{(\tau_2-\tau_1)H_0}\tau_\Phi^{\alpha'} e^{-\tau_2 H_0}\sigma_\Phi\sigma_\Phi^\dagger\rangle = G(\Delta\tau), \tag{D35}$$

$$\theta_2 \equiv \theta(\tau > 0 > \tau_1 > \tau_2): \quad \sum_{\alpha\alpha'} \langle \sigma_\Phi\sigma_\Phi^\dagger e^{\tau_1 H_0}\tau_\Phi^\alpha e^{(\tau_2-\tau_1)H_0}\tau_\Phi^{\alpha'} e^{-\tau_2 H_0}\rangle = \omega G(\Delta\tau), \tag{D36}$$

$$\theta_3 \equiv \theta(\tau > \tau_1 > \tau_2 > 0): \quad \sum_{\alpha\alpha'} \langle \sigma_\Phi e^{\tau_1 H_0}\tau_\Phi^\alpha e^{(\tau_2-\tau_1)H_0}\tau_\Phi^{\alpha'} e^{-\tau_2 H_0}\sigma_\Phi^\dagger\rangle = G(\Delta\tau), \tag{D37}$$

$$\theta_4 \equiv \theta(\tau_1 > \tau > 0 > \tau_2): \quad \sum_{\alpha\alpha'} \langle e^{\tau_1 H_0}\tau_\Phi^\alpha e^{-\tau_1 H_0}\sigma_\Phi\sigma_\Phi^\dagger e^{\tau_2 H_0}\tau_\Phi^{\alpha'} e^{-\tau_2 H_0}\rangle = \bar{\omega} G(\Delta\tau), \tag{D38}$$

$$\theta_5 \equiv \theta(\tau > \tau_1 > 0 > \tau_2): \quad \sum_{\alpha\alpha'} \langle \sigma_\Phi e^{\tau_1 H_0}\tau_\Phi^\alpha e^{-\tau_1 H_0}\sigma_\Phi^\dagger e^{\tau_2 H_0}\tau_\Phi^{\alpha'} e^{-\tau_2 H_0}\rangle = G(\Delta\tau), \tag{D39}$$

$$\theta_6 \equiv \theta(\tau_1 > \tau > \tau_2 > 0): \quad \sum_{\alpha\alpha'} \langle e^{\tau_1 H_0}\tau_\Phi^\alpha e^{-\tau_1 H_0}\sigma_\Phi e^{\tau_2 H_0}\tau_\Phi^{\alpha'} e^{-\tau_2 H_0}\sigma_\Phi^\dagger\rangle = G(\Delta\tau). \tag{D40}$$

Here, $\alpha, \alpha' = +1, -1$, and we have used the $\sigma_\Phi \tau_\Phi = \omega \tau_\Phi \sigma_\Phi$ and similar commutation relations to eliminate $\sigma_\Phi$ and $\tau_\Phi$ and express the correlators in terms of a single correlator ($\Delta\tau \equiv \tau_1 - \tau_2$):

$$G(\Delta\tau) = \sum_\alpha \sum_\Phi \prod_h \langle \exp[\Delta\tau H_0(\Phi)] \times \exp[-\Delta\tau H_0(\Phi + 2\pi\alpha)] \rangle, \quad \text{(D41)}$$

which is the correlator that was computed in the previous section. The integration over these ranges appears with an integrand that is only a function of $\tau_1 - \tau_2$. Denoting

$$I_i \equiv \int d\tau_1 d\tau_2 \theta_i G(\tau_1 - \tau_2), \quad \text{(D42)}$$

we have typical integrals of the form

$$I \sim \tau \int_0^\tau d\Delta\tau G(\Delta\tau), \quad G(\Delta\tau) \sim |\Delta\tau|^{-\kappa}, \quad \text{(D43)}$$

in terms of $\kappa$ defined before, which gives us

$$\langle \sigma_\Phi(\tau) \sigma_\Phi^\dagger(0) \rangle \sim 1 + \mathcal{C}'' \Gamma^2 \tau^{2-\kappa}, \quad \text{(D44)}$$

where $\mathcal{C}''$ is another constant. This demonstrates that the $\langle \sigma_\Phi(\tau) \sigma_\Phi(0) \rangle$ correlator disorders at the deconfinement quantum phase transition, defined by $\kappa = 2$.


[1] L. Savary and L. Balents, Quantum spin liquids: a review, Rep. Prog. Phys. **80**, 016502 (2016).

[2] Y. Zhou, K. Kanoda, and T.-K. Ng, Quantum spin liquid states, Rev. Mod. Phys. **89**, 025003 (2017).

[3] X.-G. Wen, Colloquium: Zoo of quantum-topological phases of matter, Rev. Mod. Phys. **89**, 041004 (2017).

[4] T. Senthil, A. Vishwanath, L. Balents, S. Sachdev, and M. P. A. Fisher, Deconfined quantum critical points, Science **303**, 1490 (2004).

[5] P. W. Anderson, The Resonating Valence Bond State in $La_2CuO_4$ and Superconductivity, Science **235**, 1196 (1987).

[6] Y. Kurosaki, Y. Shimizu, K. Miyagawa, K. Kanoda, and G. Saito, Mott Transition from a Spin Liquid to a Fermi Liquid in the Spin-Frustrated Organic Conductor $\kappa-(ET)_2\ Cu_2(CN)_3$, Phys. Rev. Lett. **95**, 177001 (2005).

[7] S. Yamashita, Y. Nakazawa, M. Oguni, Y. Oshima, H. Nojiri, Y. Shimizu, K. Miyagawa, and K. Kanoda, Thermodynamic properties of a spin-$\frac{1}{2}$ spin-liquid state in a $\kappa$-type organic salt, Nat. Phys. **4**, 459 (2008).

[8] P. Coleman, Y. Komijani, and E. J. König, Triplet Resonating Valence Bond State and Superconductivity in Hund's Metals, Phys. Rev. Lett. **125**, 077001 (2020).

[9] A. Dönni, G. Ehlers, H. Maletta, P. Fischer, H. Kitazawa, and M. Zolliker, Geometrically frustrated magnetic structures of the heavy-Fermion compound CePdAl studied by powder neutron diffraction, J. Phys.: Condens. Matter **8**, 11213 (1996).

[10] A. Sakai, S. Lucas, P. Gegenwart, O. Stockert, H. v. Löhneysen, and V. Fritsch, Signature of frustrated moments in quantum critical $CePd_{1-x}Ni_xAl$, Phys. Rev. B **94**, 220405(R) (2016).

[11] A. Ribak, R. M. Skiff, M. Mograbi, P. K. Rout, M. H. Fischer, J. Ruhman, K. Chashka, Y. Dagan, and A. Kanigel, Chiral superconductivity in the alternate stacking compound 4Hb-$TaS_2$, Sci. Adv. **6**, eaax9480 (2020).

[12] S. Mashhadi, Y. Kim, J. Kim, D. Weber, T. Taniguchi, K. Watanabe, N. Park, B. Lotsch, J. H. Smet, M. Burghard, and K. Kern, Spin-split band hybridization in graphene proximitized with $\alpha$-$RuCl_3$ nanosheets, Nano Lett. **19**, 4659 (2019).

[13] P. Coleman, $\frac{1}{N}$ expansion for the Kondo lattice, Phys. Rev. B **28**, 5255 (1983).

[14] D. P. Arovas and A. Auerbach, Functional integral theories of low-dimensional quantum Heisenberg models, Phys. Rev. B **38**, 316 (1988).

[15] A. M. Polyakov, Quark confinement and topology of gauge theories, Nucl. Phys. B **120**, 429 (1977).

[16] M. Hermele, T. Senthil, M. P. A. Fisher, P. A. Lee, N. Nagaosa, and X.-G. Wen, Stability of $U(1)$ spin liquids in two dimensions, Phys. Rev. B **70**, 214437 (2004).

[17] S.-S. Lee, Stability of the $U(1)$ spin liquid with a spinon Fermi surface in $2+1$ dimensions, Phys. Rev. B **78**, 085129 (2008).

[18] X.-Y. Song, C. Wang, A. Vishwanath, and Y.-C. He, Unifying description of competing orders in two-dimensional quantum magnets, Nat. Commun. **10**, 4254 (2019).

[19] X. Y. Xu, Y. Qi, L. Zhang, F. F. Assaad, C. Xu, and Z. Y. Meng, Monte Carlo Study of Lattice Compact Quantum Electrodynamics with Fermionic Matter: The Parent State of Quantum Phases, Phys. Rev. X **9**, 021022 (2019).

[20] É. Dupuis, M. B. Paranjape, and W. Witczak-Krempa, Transition from a Dirac spin liquid to an antiferromagnet: monopoles in a $QED_3$-Gross-Neveu theory, Phys. Rev. B **100**, 094443 (2019).

[21] T. Senthil, S. Sachdev, and M. Vojta, Fractionalized Fermi Liquids, Phys. Rev. Lett. **90**, 216403 (2003).

[22] Y. Komijani and P. Coleman, Model for a Ferromagnetic Quantum Critical Point in a 1$d$ Kondo Lattice, Phys. Rev. Lett. **120**, 157206 (2018).

[23] Y. Komijani and P. Coleman, Emergent Critical Charge Fluctuations at the Kondo Breakdown of Heavy Fermions, Phys. Rev. Lett. **122**, 217001 (2019).

[24] A. Stern and N. H. Lindner, Topological quantum computation-from basic concepts to first experiments, Science **339**, 1179 (2013).

[25] Ph. Nozières and A. Blandin, Kondo effect in real metals, J. Phys. France **41**, 193 (1980).

[26] N. Andrei and C. Destri, Solution of the Multichannel Kondo Problem, Phys. Rev. Lett. **52**, 364 (1984).

[27] A. M. Tsvelick and P. B. Wiegmann, Solution of the $n$-channel Kondo problem (scaling and integrability), Z. Phys. B **54**, 201 (1984).

[28] I. Affleck and A. W. W. Ludwig, Exact Critical Theory of the Two-Impurity Kondo Model, Phys. Rev. Lett. **68**, 1046 (1992).

[29] P. Coleman, L. B. Ioffe, and A. M. Tsvelik, Simple formulation of the two-channel Kondo model, Phys. Rev. B **52**, 6611 (1995).

[30] K. Ingersent, A. W. W. Ludwig, and I. Affleck, Kondo Screening in a Magnetically Frustrated Nanostructure: Exact Results on a Stable Non-Fermi-Liquid Phase, Phys. Rev. Lett. **95**, 257204 (2005).

[31] K. Hattori and H. Tsunetsugu, Non-Fermi liquid, unscreened scalar chirality, and parafermions in a frustrated tetrahedron anderson model, Phys. Rev. B **86**, 054421 (2012).

[32] B. Lazarovits, P. Simon, G. Zarand, and L. Szunyogh, Exotic Kondo Effect from Magnetic Trimers, Phys. Rev. Lett. **95**, 077202 (2005).

[33] A. K. Mitchell, T. F. Jarrold, and D. E. Logan, Quantum phase transition in quantum dot trimers, Phys. Rev. B **79**, 085124 (2009).

[34] T. Chowdhury, A. Rosch, and R. Bulla, Competition between Kondo and Kitaev physics in Kitaev clusters coupled to a Fermionic bath, Phys. Rev. B **101**, 115133 (2020).

[35] P. Zinn-Justin and N. Andrei, The generalized multi-channel Kondo model: thermodynamics and fusion equations, Nucl. Phys. B **528**, 648 (1998).

[36] P. L. S. Lopes, I. Affleck, and E. Sela, Anyons in multichannel Kondo systems, Phys. Rev. B **101**, 085141 (2020).

[37] Y. Komijani, Isolating Kondo anyons for topological quantum computation, Phys. Rev. B **101**, 235131 (2020).

[38] M. Ferrero, L. De Leo, P. Lecheminant, and M. Fabrizio, Strong correlations in a nutshell, J. Phys.: Condens. Matter **19**, 433201 (2007).

[39] A. Ramires and P. Coleman, Supersymmetric approach to heavy fermion systems, Phys. Rev. B **93**, 035120 (2016).

[40] We here use the word "spinon" synonymously with "Abrikosov fermion." Reference [90] contains a more careful terminological discussion, which illustrates that the Abrikosov fermion (called "Spinon" with capital "S" there), is not necessarily equivalent with the fermionic low-energy degrees of freedom of a spin liquid ("spinons" with lower case "s").

[41] J. B. Marston and I. Affleck, Large-$n$ limit of the Hubbard-Heisenberg model, Phys. Rev. B **39**, 11538 (1989).

[42] B. A. Jones, C. M. Varma, and J. W. Wilkins, Low-Temperature Properties of the Two-Impurity Kondo Hamiltonian, Phys. Rev. Lett. **61**, 125 (1988).

[43] B. A. Jones, B. G. Kotliar, and A. J. Millis, Mean-field analysis of two antiferromagnetically coupled Anderson impurities, Phys. Rev. B **39**, 3415 (1989).

[44] A. K. Mitchell, E. Sela, and D. E. Logan, Two-Channel Kondo Physics in Two-Impurity Kondo Models, Phys. Rev. Lett. **108**, 086405 (2012).

[45] T. Senthil, M. Vojta, and S. Sachdev, Weak magnetism and non-Fermi liquids near heavy-fermion critical points, Phys. Rev. B **69**, 035111 (2004).

[46] I. Paul, C. Pépin, and M. R. Norman, Kondo Breakdown and Hybridization Fluctuations in the Kondo-Heisenberg Lattice, Phys. Rev. Lett. **98**, 026402 (2007).

[47] M. Vojta, Orbital-selective Mott transitions: heavy fermions and beyond, J. Low Temp. Phys. **161**, 203 (2010).

[48] V. Drouin-Touchette, E. J. König, Y. Komijani, and P. Coleman, Emergent moments in a Hund's impurity, Phys. Rev. B **103**, 205147 (2021).

[49] Yu. B. Kudasov and V. M. Uzdin, Kondo State for a Compact Cr Trimer on a Metallic Surface, Phys. Rev. Lett. **89**, 276802 (2002).

[50] B. C. Paul and K. Ingersent, Frustration-induced non-Fermi-liquid behavior in a three-impurity Kondo model, arXiv preprint cond-mat/9607190 (1996).

[51] F. Eickhoff and F. B. Anders, Strongly correlated multi-impurity models: the crossover from a single-impurity problem to lattice models, Phys. Rev. B **102**, 205132 (2020).

[52] P. P. Baruselli, R. Requist, M. Fabrizio, and E. Tosatti, Ferromagnetic Kondo Effect in a Triple Quantum Dot System, Phys. Rev. Lett. **111**, 047201 (2013).

[53] K. P. Wójcik, I. Weymann, and J. Kroha, Magnetic Kondo regimes in a frustrated half-filled trimer, Phys. Rev. B **102**, 045144 (2020).

[54] A. M. Tsvelick, The thermodynamics of multichannel Kondo problem, J. Phys. C **18**, 159 (1985).

[55] I. Affleck, Lectures given at the 35th Cracow school of theoretical physics, Zakopane, Poland, june 1995, Acta Polon. B **26**, 1869 (1995).

[56] A. Jerez, N. Andrei, and G. Zaránd, Solution of the multichannel Coqblin-Schrieffer impurity model and application to multilevel systems, Phys. Rev. B **58**, 3814 (1998).

[57] P. Coleman, J. B. Marston, and A. J. Schofield, Transport anomalies in a simplified model for a heavy-electron quantum critical point, Phys. Rev. B **72**, 245111 (2005).

[58] X.-G. Wen, Quantum orders and symmetric spin liquids, Phys. Rev. B **65**, 165113 (2002).

[59] E. J. König, P. Coleman, and A. M. Tsvelik, Soluble limit and criticality of fermions in $\mathbb{Z}_2$ gauge theories, Phys. Rev. B **102**, 155143 (2020).

[60] I. Affleck and A. W. W. Ludwig, Universal Noninteger "Ground-State Degeneracy" in Critical Quantum Systems, Phys. Rev. Lett. **67**, 161 (1991).

[61] O. Narayan and B. S. Shastry, The 2D Coulomb gas on a 1D lattice, J. Phys. A: Math. Gen. **32**, 1131 (1999).

[62] A. O. Caldeira and A. J. Leggett, Quantum tunnelling in a dissipative system, Ann. Phys. **149**, 374 (1983).

[63] C. L. Kane and M. P. A. Fisher, Transport in a One-Channel Luttinger Liquid, Phys. Rev. Lett. **68**, 1220 (1992).

[64] J. Villain, A magnetic analogue of stereoisomerism: application to helimagnetism in two dimensions, J. Phys. **38**, 385 (1977).

[65] E. Fradkin and L. Susskind, Order and disorder in gauge systems and magnets, Phys. Rev. D **17**, 2637 (1978).

[66] P. Chandra, P. Coleman, and A. I. Larkin, Ising Transition in Frustrated Heisenberg Models, Phys. Rev. Lett. **64**, 88 (1990).

[67] R. M. Fernandes, P. P. Orth, and J. Schmalian, Intertwined vestigial order in quantum materials: nematicity and beyond, Annu. Rev. Condens. Matter Phys. **10**, 133 (2019).

[68] S. Sachdev, Topological order, emergent gauge fields, and fermi surface reconstruction, Rep. Prog. Phys. **82**, 014001 (2018).

[69] B. Béri and N. R. Cooper, Topological Kondo Effect with Majorana Fermions, Phys. Rev. Lett. **109**, 156803 (2012).

[70] E. J. König, P. Coleman, and A. M. Tsvelik, Spin magnetometry as a probe of stripe superconductivity in twisted bilayer graphene, Phys. Rev. B **102**, 104514 (2020).

[71] A. Georges, G. Kotliar, W. Krauth, and M. J. Rozenberg, Dynamical mean-field theory of strongly correlated fermion systems and the limit of infinite dimensions, Rev. Mod. Phys. **68**, 13 (1996).

[72] T. Maier, M. Jarrell, T. Pruschke, and M. H. Hettler, Quantum cluster theories, Rev. Mod. Phys. **77**, 1027 (2005).

[73] A. Keselman, B. Bauer, C. Xu, and C.-M. Jian, Emergent Fermi Surface in a Triangular-Lattice $SU(4)$ Quantum Antiferromagnet, Phys. Rev. Lett. **125**, 117202 (2020).

[74] A. Wietek, R. Rossi, F. Simkovic IV, M. Klett, P. Hansmann, M. Ferrero, E. M. Stoudenmire, T. Schäfer, and A. Georges, Mott insulating states with competing orders in the triangular lattice Hubbard model, arXiv preprint arXiv:2102.12904 (2021).

[75] C. Xu and L. Balents, Topological Superconductivity in Twisted Multilayer Graphene, Phys. Rev. Lett. **121**, 087001 (2018).

[76] M. Haule, E. Y. Andrei, and K. Haule, The Mott-semiconducting state in the magic angle bilayer graphene, arXiv:1901.09852 (2019).

[77] S. K. Pati, R. R. P. Singh, and D. I. Khomskii, Alternating Spin and Orbital Dimerization and Spin-Gap Formation in Coupled Spin-Orbital Systems, Phys. Rev. Lett. **81**, 5406 (1998).

[78] Y. Q. Li, M. Ma, D. N. Shi, and F. C. Zhang, SU(4) Theory for Spin Systems with Orbital Degeneracy, Phys. Rev. Lett. **81**, 3527 (1998).

[79] Y. Tokura and N. Nagaosa, Orbital physics in transition-metal oxides, Science **288**, 462 (2000).

[80] M. G. Yamada, M. Oshikawa, and G. Jackeli, Emergent $SU(4)$ Symmetry in $\alpha$-$ZrCl_3$ and Crystalline Spin-Orbital Liquids, Phys. Rev. Lett. **121**, 097201 (2018).

[81] A. V. Gorshkov, M. Hermele, V. Gurarie, C. Xu, P. S Julienne, J. Ye, P. Zoller, E. Demler, M. D Lukin, and A. M. Rey, Two-orbital $SU(n)$ magnetism with ultracold alkaline-earth atoms, Nat. Phys. **6**, 289 (2010).

[82] F. Scazza, C. Hofrichter, M. Höfer, P. C. De Groot, I. Bloch, and S. Fölling, Observation of two-orbital spin-exchange interactions with ultracold $SU(n)$-symmetric fermions, Nat. Phys. **10**, 779 (2014).

[83] A. J. Keller, S. Amasha, I. Weymann, C. P. Moca, I. G. Rau, J. A. Katine, H. Shtrikman, G. Zaránd, and D. Goldhaber-Gordon, Emergent $SU(4)$ Kondo physics in a spin–charge-entangled double quantum dot, Nat. Phys. **10**, 145 (2014).

[84] M. Seo, H. K. Choi, S.-Y. Lee, N. Kim, Y. Chung, H.-S. Sim, V. Umansky, and D. Mahalu, Charge Frustration in a Triangular Triple Quantum Dot, Phys. Rev. Lett. **110**, 046803 (2013).

[85] Z. Iftikhar, A. Anthore, A. K. Mitchell, F. D. Parmentier, U. Gennser, A. Ouerghi, A. Cavanna, C. Mora, P. Simon, and F. Pierre, Tunable quantum criticality and super-ballistic transport in a charge Kondo circuit, Science **360**, 1315 (2018).

[86] P. Coleman, *Introduction to Many-Body Physics* (Cambridge University Press, Cambridge, 2015).

[87] A. I. Vaĭnshteĭn, V. I. Zakharov, V. A. Novikov, and M. A. Shifman, ABC of instantons, Soviet Physics Uspekhi **25**, 195 (1982).

[88] A. O. Gogolin, A. A. Nersesyan, and A. M. Tsvelik, *Bosonization and Strongly Correlated Systems* (Cambridge University Press, Cambridge, 2004).

[89] I. Affleck and A. W. W. Ludwig, The Fermi edge singularity and boundary condition changing operators, J. Phys. A: Math. Gen. **27**, 5375 (1994).

[90] T. Senthil and M. P. A. Fisher, Fractionalization and confinement in the $U(1)$ and $\mathbb{Z}_2$ gauge theories of strongly correlated systems, J. Phys. A: Math. Gen. **34**, L119 (2001).